

Doppler Radar Wind Profiles

Iwan Holleman

Scientific Report, KNMI WR-2003-02, 2003

Contents

1	Introduction	5
2	Settings of Doppler Radar	9
2.1	Doppler Effect	9
2.2	Coherent Receiver	10
2.3	Doppler Power Spectrum	12
2.4	Clutter Filtering	15
2.5	Pulse-Pair Processing	17
2.6	Doppler Radar Scan Strategy	18
3	Methods for Wind Profile Retrieval	25
3.1	Radial Velocity from Local Wind Model	25
3.2	Velocity Azimuth Display	28
3.3	Volume Velocity Processing	30
3.4	Sources of Error	32
3.5	Implementation	34
4	Intercomparison of Wind Profile Retrieval Techniques	37
4.1	Available Wind Profile Data	37
4.2	Doppler Wind Profiles against Radiosonde	38
4.3	Doppler Wind Profiles against Hirlam	42
4.4	Rejection of Radial Velocity Outliers	44
5	Performance of VVP Retrieval Technique	47
5.1	Availability of Wind Profiles	47
5.2	Quality as a function of Wind Speed	49
5.3	Quality as a function of Height	51
5.4	Removal of Elevations	58
5.5	Outliers: Bird Migration?	60
6	Conclusions and Recommendations	65

Chapter 1

Introduction

Upper-air wind observations are of crucial importance for general (operational) meteorology, nowcasting, aviation meteorology, and numerical weather prediction. On the synoptic scale dynamical weather phenomena are mainly determined by the wind field aloft, and on the mesoscale the degree of organization of thunderstorms is determined by the vertical wind shear and helicity (Holton, 1992). In the WMO guide on Meteorological Instruments and Methods of Observation, a chapter has been dedicated to measurement of upper-air wind (WMO, 1996). Furthermore, the importance of upper-air wind forces many meteorological institutes to launch radiowind sondes, designated to measure upper-air wind only, in between the radiosonde observations.

Apart from radiowind or radiosonde, many other (remote sensing) techniques are available to measure the upper-air wind. Observations by ascending, descending, and cruising airplanes, AMDARs, are nowadays a valuable source of upper-air wind data. Ground-based remote sensing techniques for observation of wind profiles, like sodar, wind profiler, and lidars, are used operationally or are being developed for operational use. Satellite systems can be used for upper-air wind observations as well. Cloud-motion vectors, a measure for upper-air wind, are deduced from sequences of infrared images from the geostationary Meteosat and assimilated in operational Numerical Weather Prediction (NWP) models. In addition, ESA has planned an Atmospheric Dynamics Mission (ADM) which will be launched in 2006 and will measure wind profiles using the lidar technique.

At KNMI scientific work focused on several of these techniques for obtaining upper-air wind data is ongoing. The Quality Evaluation Centre (QEVC) for E-AMDAR observations is hosted by KNMI and quarterly reports on quality and availability of the observations are produced (Meulen, 2003). At the Cabauw remote sensing site, a boundary layer wind profiler is stationed and a long-term intercomparison with tower measurements has been performed by Klein Baltink (1998). The potential impact of a network of boundary layer wind profilers and sodars for mesoscale wind analysis in the Netherlands has been assessed by the ASWAN project (Tijm and Wu, 2000). Dlhopolsky and Feijt (2003) have investigated the representative heights

for atmospheric motion vectors deduced from Meteosat. KNMI takes part in the development of ADM and Observation System Simulation Experiments (OSSEs) are performed by Marseille and Stoffelen (2003).

Doppler weather radars are also capable of providing upper air wind observations using dedicated methods for retrieval of wind profiles. In the early sixties, Lhermitte and Atlas (1961) and Browning and Wexler (1968) introduced the Velocity-Azimuth Display (VAD) technique for the extraction of upper-air wind data from Doppler radar observations. When using the VAD technique, it is not possible to separate the contributions of the vertical velocity, which is a sum of the vertical wind velocity and the hydrometeor fall velocity, and the divergence of the horizontal wind field to the offset of the VAD. Improved versions of the VAD technique, which are mainly designed to separate these two contributions, were developed in the late eighties and early nineties and have been dubbed the Extended-VAD (EVAD) technique (Srivastava et al., 1986; Matejka and Srivastava, 1991) and the Concurrent-Extended-VAD (CEVAD) technique (Matejka, 1993). Instead of processing a single VAD or a series of VADs, one can also process all available volume scan data in a certain height layer at once using a multi-dimensional linear regression. This so-called Volume Velocity Processing technique (VVP) has been introduced by Waldteufel and Corbin (1979). Nowadays, both the VAD technique and the VVP technique are widely used to retrieve wind profiles from Doppler radar observations.

Despite the widespread use of the VAD and VVP retrieval techniques, only a few verification or case studies with the retrieved wind profiles have been published so far and no intercomparison study between VAD and VVP retrieved horizontal wind data has been published up to now. Andersson (1998) has published verification results of VAD wind profiles against those from radiosonde and the Hirlam model. Both the availability and the accuracy of the VAD wind vectors of the Swedish weather radars were investigated. The availability of the VAD wind vectors is about 80% at 925 hPa, and it drops to about 15% at 400 hPa. The rms vector differences between the VAD wind vectors and the radiosonde wind vectors is about 3 m/s. The EVAD technique has been used to study the trailing anvil region associated with a squall line (Srivastava et al., 1986). Profiles of wind speed and direction, hydrometeor fall speed, and divergence have been obtained. Details of the kinematic structure of the mid-latitude squall line are revealed by this Doppler radar study. Xin and Reuter (1998) have investigated how the number of VVP parameters affects the accuracy of the retrieved parameters and have applied the optimized VVP technique to an Alberta storm. It is concluded that the initiation and enhancement of precipitating cells were associated with the VVP low-level convergence. An interesting intercomparison of divergence and vertical velocity obtained by (C)EVAD, and VVP techniques is presented by Cifelli et al. (1996). The performance of the techniques were quite similar, although the VVP profiles often extended to greater heights. Unfortunately, no intercomparison of the retrieved wind speeds and directions was made. Boccippio (1995) has performed a diagnostic analysis of the VVP retrieval technique and he has developed an algorithm for preparation and analysis of a robust VVP retrieval.

An important application of (Doppler radar) wind profiles is the assimilation in operational

NWP models. The European Union COST-717 program on “Use of radar observations in hydrological and NWP models” deals amongst other things with quality control and assimilation of Doppler radar wind profiles and radial velocity data in NWP models (Rossa, 2000). As part of this program, Linsdskog et al. (2002) have compared the relative impact of assimilating VAD-wind profiles and radial wind super-observations in the Hirlam model. The benefits to the model forecast were found to be comparable for both types of wind information. At the National Centers for Environmental Prediction (NCEP) assimilation of VAD wind profiles from the WSR-88D radars started in 1997, but soon many problems with the data became evident and the operational assimilation was ended in 1999 (Collins, 2001). A quality control procedure for VAD profiles has been developed which removes wind vectors with very small magnitude, clear outliers, and “wind” vectors due to migrating birds. The VAD profiles were re-admitted operationally in 2000 (Collins, 2001). Within the framework of the Eumetnet WINPROF program on wind profilers, a wind profile database and quality control center (CWINDE) is operated by the UK Met Office (CWINDE, 2003). Both wind profiler and Doppler radar wind profiles are collected and processed by the CWINDE hub. The quality control is performed by a verification against the UK regional model. Monthly reports on the availability and quality of the profiles are produced for all sites sending data to the hub.

In this scientific report, an intercomparison of different implementations of the VAD and VVP retrieval techniques and an extensive verification of Doppler radar VVP wind profiles against radiosonde and Hirlam model profiles are presented. Nine months of wind profile data have been used for the intercomparison and verification. Modules to retrieve wind profiles from Doppler volume scan data using different implementations of the VAD and VVP techniques have been developed, but wind profiles from the Rainbow VVP module (Gematronik, 2003) have been considered as well. It is concluded that the VVP retrieval technique provides wind profiles with a higher availability and a better quality than the VAD technique. In addition, it is found that the most simple implementation of the VVP technique, i.e., with the fewest wind field parameters, provides the best horizontal wind data. The verification results indicate that the accuracy of the VVP wind profiles generally satisfies the requirements for upper-air wind measurements as provided by WMO (1996). Recommendations for improvement of the Rainbow VVP module (Gematronik, 2003) which will be used operationally at KNMI are made. The outline of the remaining of the report is as follows:

- In chapter 2 an introduction to Doppler radar velocity measurements is given and the relevant settings of the Doppler radar system are discussed. In addition, a couple of experiments are presented which aided in finalizing the settings of the Doppler processing.
- The basic principles behind the Doppler radar wind profile retrieval techniques are introduced in chapter 3. The VAD and VVP retrieval techniques are described and different implementations of the techniques are discussed.
- In chapter 4 the results from the intercomparison of VAD and VVP retrieval techniques and the different implementations are presented.

- An extensive evaluation of the performance of the VVP retrieval technique is presented in chapter 5. Both the availability and the quality of the retrieved wind vectors are analyzed and discussed in detail.
- In the last chapter the conclusions from the intercomparison and verification are summarized and recommendations for further application are made.

Chapter 2

Settings of Doppler Radar

2.1 Doppler Effect

A Doppler weather radar is capable of determining one component of the velocity of scattering particles. Only the velocity component along the line of sight, the so-called radial velocity, can be determined. A Doppler radar is commonly associated with measurements of frequency shifts, because of the low velocities of hydrometeors, however, these shifts cannot be observed directly. The phase of the scattered electromagnetic waves is employed to determine the Doppler frequency shift instead. The received phase ϕ from an electromagnetic wave scattered at range R from the radar is given by:

$$\phi = 2\pi \frac{2R}{\lambda} \quad (2.1)$$

where λ is the wavelength of the electromagnetic waves. The Doppler frequency shift f_d is related to the rate of phase change:

$$f_d = \frac{1}{2\pi} \frac{d\phi}{dt} = \frac{2V_r}{\lambda} \quad (2.2)$$

where the radial velocity V_r is defined as the derivative of the range with respect to time. This equation for the Doppler frequency shift can also be deduced by applying the classical Doppler effect to scattering from a moving target. For a hydrometeor with a radial velocity of 10 m/s observed with a C-band radar ($\lambda = 5.3$ cm), the Doppler frequency shift is roughly 400 Hz which is about seven orders of magnitude smaller than the radar frequency.

A pulsed Doppler radar transmits a sequence of electromagnetic pulses and receives the scattered signal in between. Typically the transmitted pulses have a power of 250 kW and a duration of 0.5 μ s. Most operational Doppler radars transmit an equidistant sequence with separation given by the pulse repetition time T , which is typically on the order of 1 ms. For each range bin, the phase of the received electromagnetic waves is monitored from pulse to

pulse. The difference between phases from two subsequent pulses $\Delta\phi$ is directly related to the radial velocity:

$$\Delta\phi = 2\pi \frac{2V_r T}{\lambda} \quad (2.3)$$

It will be detailed below that the retrieval of the (average) radial velocity and spectral width from the received electromagnetic waves is not this straightforward, but this equation presents the basic principle. The maximum phase difference that can be determined unambiguously is limited to $\pm\pi$, and therefore the radial velocity has a maximum unambiguous value as well. The maximum unambiguous radial velocity is given by:

$$V_r^u = \frac{\lambda}{4T} = \frac{\lambda \text{ PRF}}{4} \quad (2.4)$$

where PRF is the Pulse Repetition Frequency. For a typical C-band Doppler radar using a pulse repetition time of 1 ms or equivalently a PRF of 1 kHz, the maximum unambiguous velocity is equal to 13 m/s.

2.2 Coherent Receiver

A pulsed Doppler weather radar can either be “fully coherent” or “coherent on receive”. In the former case, the transmitter is based on a klystron and therefore the phase of each pulse can be controlled. The WSR-88D weather radars in the NEXRAD network (Serafin and Wilson, 2000), for example, are fully coherent. In the latter case, the transmitter is based on a magnetron and therefore the phase of each pulse is fully random. Most operational Doppler weather radars in Europe, including those of KNMI, are coherent on receive (Meischner et al., 1997). A klystron-based receiver is more expensive, but offers higher (phase) stability and reliability. On the other hand, a magnetron-based radar has hardly any problems with second-trip echoes (range aliasing) due to the incoherent nature of the transmitted pulses.

A simplified overview of a coherent on receive Doppler radar is depicted in figure 2.1. The transmitted pulses are generated by a magnetron and are fed into the radar antenna via a transmit-receive coupler. The phase of the transmitted pulse is monitored and used to start the stable local oscillator (STALO). The STALO provides two reference signals: one in phase with the transmitted pulse and one 90 degrees out of phase. The received signal, or echo, $E(t)$ can be represented by:

$$E(t) = \bar{E}(t) \sin(\omega t + \phi(t)) \quad (2.5)$$

with $\bar{E}(t)$ the (time-dependent) amplitude of the echo, ω the angular frequency of the electromagnetic wave, and $\phi(t)$ the phase shift with respect to the transmitted wave. An in-phase signal $I(t)$ and a quadrature signal $Q(t)$ are generated by multiplying the received signal with

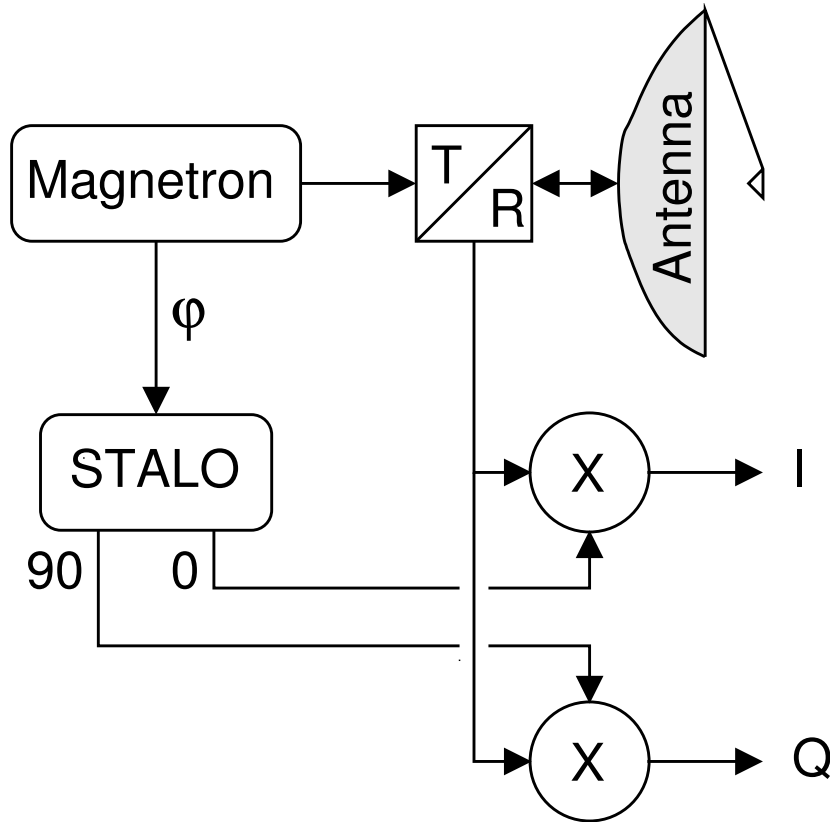


Figure 2.1: A simplified overview of a coherent on receive Doppler weather radar. The connections between the magnetron, transmit-receive coupler (T/R), antenna, stable local oscillator (STALO), and the down-converter (X) for the in-phase (I) and quadrature phase (Q) outputs are shown.

the in-phase ($\sin(\omega t)$) and out-of-phase ($\cos(\omega t)$) signals of the STALO, respectively, and averaging of the result over many wave cycles. In mathematical formulation this down-conversion process is described by:

$$I(t) \equiv \frac{\omega}{\pi} \int_0^{2\pi/\omega} E(t) \sin(\omega t) dt \simeq \bar{E}(t) \cos \phi(t) \quad (2.6)$$

$$Q(t) \equiv \frac{\omega}{\pi} \int_0^{2\pi/\omega} E(t) \cos(\omega t) dt \simeq \bar{E}(t) \sin \phi(t) \quad (2.7)$$

It is evident that the amplitude and phase of the echo can be deduced from the in-phase and quadrature-phase signals. The averaging period depends on the desired range resolution, but is typical on the order of $1 \mu s$. For weather echoes, the $I(t)$ and $Q(t)$ signals are uncorrelated and have a Gaussian distribution (Doviak and Zrnić, 1993).

It has been detailed in the previous section that the radial velocity can be deduced from evo-

lution of the phase of the received signal during subsequent pulses. The in-phase and quadrature phase signals contain information on this phase evolution. The time coordinate of the $I(t)$ and $Q(t)$ signals is primarily related to the range of the scatterers from the radar. After a time T , equal to the pulse repetition time, the signals are primarily related to the echoes of the next transmitted pulse. During Doppler processing the $I(t)$ and $Q(t)$ signals are analyzed at constant range and sampled by each transmitted pulse. It is convenient to combine the $I(t)$ and $Q(t)$ signal to one complex quantity:

$$Z(n) \equiv I(nT) + i Q(nT) \quad (2.8)$$

where $Z(n)$ is the complex signal at a certain range for transmitted pulse n . During Doppler signal processing a series of $Z(n)$ values is analyzed for each range bin.

The evolution of the amplitude and phase of the complex signal as a function of pulse number is determined using autocorrelation. The autocorrelation function $R(l)$ is calculated from the complex signal $Z(n)$:

$$R(l) \equiv \frac{1}{N - |l|} \sum_{n=0}^{N-|l|-1} Z^*(n) Z(n + l) \quad (2.9)$$

In this equation N represents the number of transmitted pulses used to calculate the autocorrelation function and l is the lag of the autocorrelation. For a lag $l = 0$ the autocorrelation is equal to the intensity of the received signal, while the autocorrelation for lags of 1 and 2 can be used to extract the mean radial velocity and the spectral width. From the autocorrelation, the power spectrum $S(f)$, also known as periodogram, can be obtained using a discrete Fourier transform (DFT):

$$S(f) \equiv T \sum_{l=-N+1}^{N-1} R(l) \exp(-i2\pi lf) \quad (2.10)$$

From a signal processing point of view it is important to note that the power spectrum can also be obtained directly from the complex signal $Z(n)$ using DFT (Doviak and Zrnić, 1993). The frequency axis of the power spectrum is proportional to the radial velocity and can directly be converted using equation 2.2. The power spectrum of the received signal is a power-weighted distribution of the radial velocities of the scatterers (Doviak and Zrnić, 1993). This “Doppler spectrum” plays a key role in the understanding and processing of Doppler radar observations.

2.3 Doppler Power Spectrum

The Doppler spectrum or power spectrum contains the information on the distribution of radial velocities of the meteorological scatterers in the power-weighted measurement volume. From the shape of the Doppler spectrum, the hydrometeor parameters, most notably the mean radial

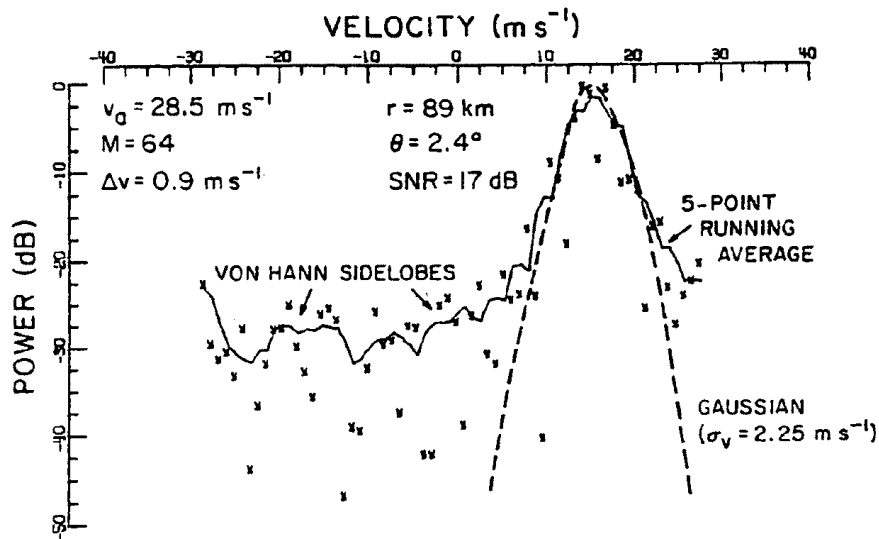


Figure 2.2: A typical Doppler spectrum for a resolution volume within a thunderstorm. This spectrum is obtained from a Fourier transform using 64 samples and a von Hann window. This figure is taken from Doviak and Zrnić (1993).

velocity and spectral width, can be deduced. In figure 2.2 an example of a Doppler spectrum from hydrometeor scatterers is depicted. It will be detailed below that the Doppler processing used at KNMI does not allow for extraction of the power spectrum, and therefore the figure is taken from Doviak and Zrnić (1993). The unambiguous velocity interval of this Doppler spectrum is ± 28.5 m/s and the received power for each velocity bin is given in decibel relative to the peak power. The Doppler spectrum has a clear maximum around a velocity of 15 m/s which is equal to the mean radial velocity. The spectral width of 2.2 m/s is determined from a Gaussian fit to the power spectrum. In addition it is evident from the figure that the noise level is about 25 dB below the peak power. Ground clutter, i.e., signal from fixed non-hydrometeor targets, can easily be recognized from a Doppler spectrum. An example of a Doppler spectrum of ground clutter is depicted in figure 2.3 which again is taken from Doviak and Zrnić (1993). It is obvious that ground clutter produces a narrow peak centered around zero velocity. The spectral width of this clutter peak is only 0.45 m/s and it is thus a factor of four smaller than that of the hydrometeor peak.

For a Doppler weather radar at least three types of contributions to the power spectrum can be distinguished: noise, ground clutter, and hydrometeor signal. The relative importance of each of these contributions depends on the range from the radar and the actual meteorological circumstances. In order to process the received Doppler signal assumptions on the spectral shape of these contributions have to be made. For white noise the power spectrum is constant

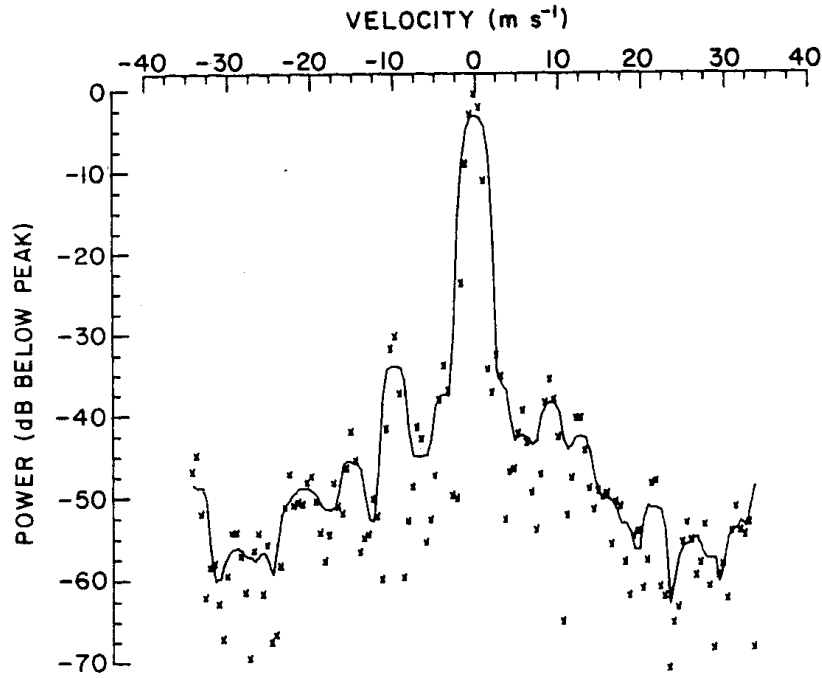


Figure 2.3: A Doppler spectrum of ground clutter for an antenna scanning at 10 degree/s. The Doppler processing is similar that of the data in figure 2.2. The ground clutter peak is centered at zero velocity and its spectral width is only 0.45 m/s. This figure is taken from Doviak and Zrnić (1993).

and equal to:

$$S(f) \equiv TN_0 \quad (2.11)$$

$$R(n) = \begin{cases} N_0 & \text{for } n = 0 \\ 0 & \text{for } n \neq 0 \end{cases} \quad (2.12)$$

where N_0 is the noise power. The corresponding autocorrelation function for white noise is obtained via an inverse discrete Fourier transform. The autocorrelation function is zero for $n \neq 0$ reflecting that white noise is completely uncorrelated. The power spectrum of a ground clutter signal can be approximated by a Gaussian function centered around zero frequency:

$$S(f) \equiv \frac{C_0}{\sigma_c \sqrt{2\pi}} \exp(-f^2/(2\sigma_c^2)) \quad (2.13)$$

$$R(n) = C_0 \exp(-(2\pi n T \sigma_c)^2/2) \quad (2.14)$$

In these equations for the power spectrum and the autocorrelation function, C_0 and σ_c represent the power and the spectral width, respectively, of the ground clutter signal. For a hydrometeor

scattering signal, the power spectrum is well approximated by a Gaussian function centered on the mean Doppler frequency shift f_d . Using equation 2.2 this frequency shift can be converted to the mean radial velocity of the scattering hydrometeors. The power spectrum and autocorrelation function for the hydrometeor signal are described by:

$$S(f) \equiv \frac{S_0}{\sigma\sqrt{2\pi}} \exp(-(f - f_d)^2/(2\sigma^2)) \quad (2.15)$$

$$R(n) = S_0 \exp(i2\pi n T f_d) \exp(-(2\pi n T \sigma)^2/2) \quad (2.16)$$

where S_0 is the scattered power and σ is the spectral width. Any Doppler spectrum can be described by a linear combination of the preceding contributions. As a matter of fact this also holds true for the autocorrelation functions, because the conversion between power spectral and autocorrelation is linear (DFT). It will be detailed below that this property of the autocorrelation function is employed during Doppler pulse-pair processing.

2.4 Clutter Filtering

As implied by its name clutter is an unwanted signal in Doppler radar observations of reflectivity factor and mean velocity. Clutter may be caused by scattering of the antenna sidelobe power from ground surface, by (partial) beam blockage, by anomalous propagation followed by scattering from ground or sea surface, or by scattering from non-hydrometeor scatterers in the atmosphere. Clutter from ground targets, so-called ground clutter, is infamous for causing spurious echoes in weather radar reflectivity images, but it also affects the quality of mean radial velocity observations. Seltmann (2000) has shown that ground clutter superimposed on a hydrometeor signal leads to lower signal quality and a bias towards zero of the mean radial velocity. Ground clutter interference in the Doppler signal $Z(n)$ is suppressed, however, by digital filtering in the time or frequency domain.

It has been shown in figure 2.3 that ground clutter gives rise to a narrow peak around zero frequency in the Doppler spectrum. This low frequency component can be removed from the Doppler signal by applying a sharp high-pass filter. Digital filtering of the Doppler signal can either be done in the frequency domain or in the time domain. In the former case the power spectrum is calculated, subsequently a window function is applied, and finally the spectrum around zero frequency is reconstructed using interpolation (Sigmet, 1998). In the latter case filtered signal $\tilde{Z}(n)$ is given by:

$$\tilde{Z}(n) = \sum_{m=0}^M b_m Z(n-m) - \sum_{m=1}^M c_m \tilde{Z}(n-m) \quad (2.17)$$

where M is the order of the time domain filter. It is evident that the filtered signal is a linear combination of the (un)filtered signals at previous time steps. When all coefficients c_m are

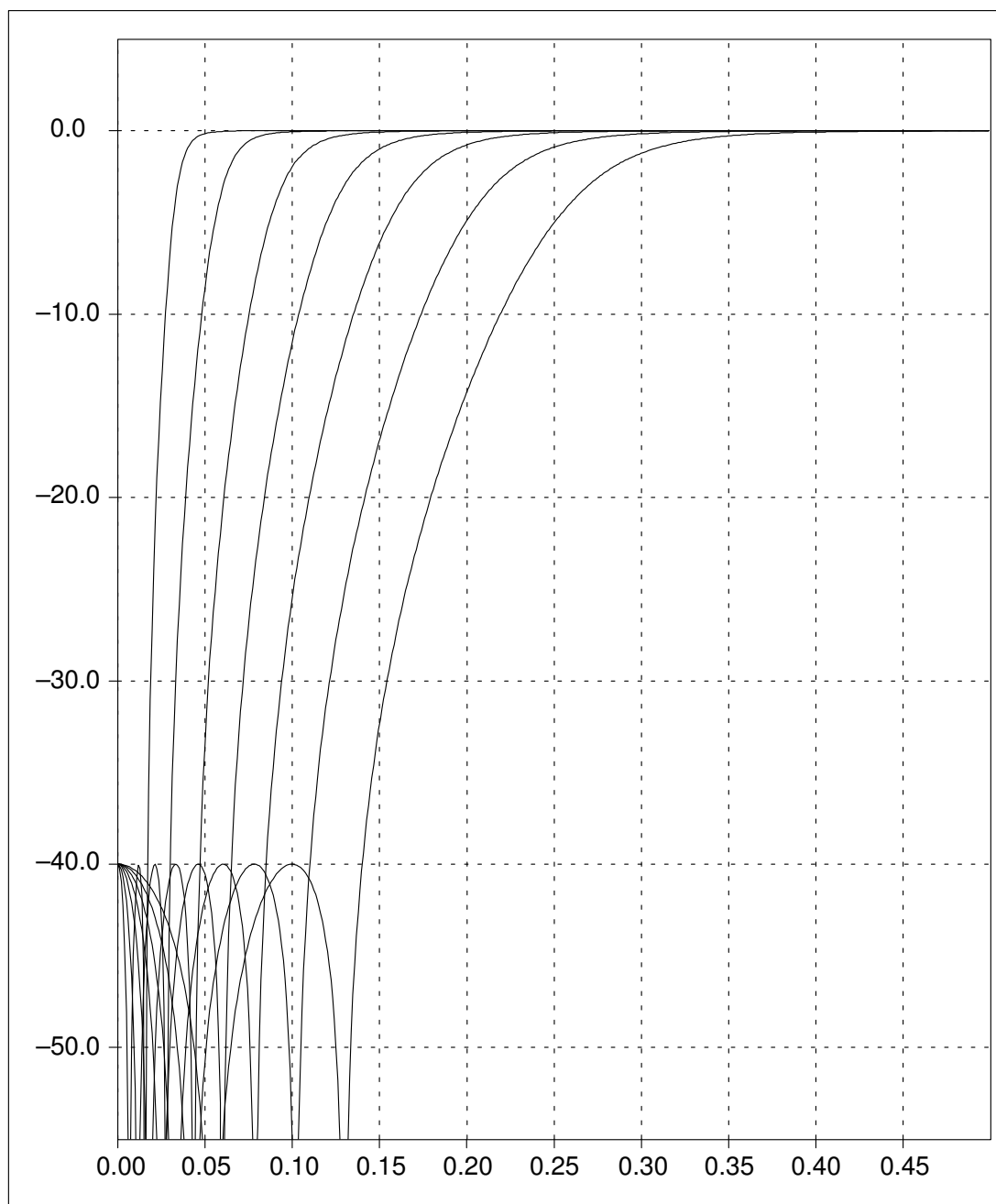


Figure 2.4: Filter characteristics of digital Infinite Impulse Response high-pass clutter filters with 40 dB attenuation. These filters are preprogrammed in the RVP6 signal processor. The horizontal axis represents the radial velocity scaled to the unambiguous velocity and the vertical axis the attenuation in dB. This figure is taken from Sigmet (1998).

zero the filter is a so-called finite impulse response filter (FIR), and else it is a so-called infinite impulse response filter (IIR). More information on digital filtering in the time domain can be found in Press et al. (1992). The filter characteristics or filter function depends on the choice of coefficients b_m and c_m .

The RVP6 Doppler Signal Processor (Sigmet Inc.) is shipped with fourteen sets of preprogrammed coefficients for fourth-order IIR filtering: seven sets for 40 dB ground clutter suppressing and seven sets for 50 dB suppression (Sigmet, 1998). In figure 2.4 the filter functions of the seven 40 dB clutter filters are depicted. The horizontal axis represents the frequency or radial velocity scaled to the unambiguous one and the vertical axis gives the suppression of the filter in dB. It is evident that the cut-off frequency and “tail” of the seven high-pass filters are different. The filter functions of the 50 dB clutter filters (not shown) have a much longer tail than the corresponding 40 dB filters, which is the cost of the higher suppression. It is important to note that, in contrast to frequency domain filtering, time domain filtering does not allow for reconstruction of the power spectrum around zero frequency. Given the higher computational demand for frequency domain filtering and the amount of Doppler data to be processed, our current signal processors can only handle time domain filtering.

2.5 Pulse-Pair Processing

The pulse-pair method is a widely used method for estimation of the mean radial velocity and spectral width of Doppler spectra in the time domain. One of the first articles that presents an extensive description and analysis of the pulse-pair method is written by Srivastava et al. (1979). The pulse-pair method assumes that the noise is truly white and uncorrelated from the signal. In addition, the method assumes that the power spectrum can be approximated by a single Gaussian function. It is crucial that a possible ground clutter peak is removed from the Doppler signal by time or frequency domain filtering before pulse-pair processing is applied. The presence of ground clutter will result in a bias of the estimated mean radial velocity towards zero (Seltmann, 2000).

Assuming that the power spectrum consists of white noise and a single Gaussian function from hydrometeor scattering, equations 2.12 and 2.16 can be used to calculate the approximate autocorrelation function at the zeroth, first, and second lags:

$$R(0) = S_0 + N_0 \quad (2.18)$$

$$R(1) = S_0 \exp(i2\pi T f_d) \exp(-(2\pi T \sigma)^2/2) \quad (2.19)$$

$$R(2) = S_0 \exp(i4\pi T f_d) \exp(-2(2\pi T \sigma)^2) \quad (2.20)$$

The autocorrelation function at zeroth lag $R(0)$ is equal to the received power and is in principle only of importance for reflectivity factor measurements. The mean radial velocity can be

estimated from the autocorrelation function at the first lag:

$$V_r = \frac{\lambda f_d}{2} = \frac{\lambda}{4\pi T} \arg(R(1)) \quad (2.21)$$

It is important to note that this estimation of the mean radial velocity is unbiased by white noise and unbiased for symmetric Doppler spectra (Passarelli Jr. and Siggia, 1983). For high signal-to-noise ratios ($S_0 \gg N_0$), the spectral width can be estimated using just the zeroth and first lag of the autocorrelation function. A more accurate approach is to use the autocorrelation function at the first and second lag to calculate the spectral width:

$$W = \frac{\lambda\sigma}{2} = \frac{\lambda}{2\pi\sqrt{6T}} \sqrt{\ln\left(\frac{|R(1)|}{|R(2)|}\right)} \quad (2.22)$$

where W is the spectral width in m/s. It has been detailed in section 2.2 that the autocorrelation function at a certain lag can be obtained from the received Doppler signal. By insertion of the obtained autocorrelation at zeroth, first, and second lags into the preceding equations, the mean radial velocity and the spectral width can be extracted from the received signal. This type of pulse-pair processing is integrated in the RVP6 Doppler signal processors which are used at KNMI.

Apart from deriving the reflectivity factor, the mean radial velocity, and the spectral width, the RVP6 processor has the ability to accept or reject range bins based on threshold qualifiers derived from the received signal (Sigmet, 1998). The type of threshold qualifiers used for the quality control of the range bins depends on the output parameter. For mean radial velocity a Signal Quality Index and a Clutter Correction threshold can be applied, and for spectral width an additional Weather Signal Power threshold is available. The Signal Quality Index (SQI) is defined as the ratio of the autocorrelation at the zeroth and first lags:

$$\text{SQI} \equiv \frac{|R(1)|}{R(0)} = \frac{S_0}{N_0 + S_0} \exp(-(4\pi TW)^2/(2\lambda^2)) \quad (2.23)$$

and is always between zero and one. The SQI threshold qualifier is a combination of signal-to-noise ratio and spectral width and thus is a measure of the spectral brightness of the Doppler signal. The Clutter Correction (CCOR) threshold is defined as the ratio of the autocorrelation function at lag zero after clutter filtering and that before filtering. The CCOR factor is given in dB and is also used to correct the reflectivity signal from the LOG channel. Finally, the Weather Signal Power (SIG) is defined as the ratio (in dB) of signal power S_0 and the noise power N_0 .

2.6 Doppler Radar Scan Strategy

KNMI operates two identical C-band Doppler weather radars. In this study volume data from the radar in De Bilt and processed wind profiles from both radars have been used. The De

Table 2.1: Settings of De Bilt and Den Helder radars for dedicated Doppler scan. This scan is repeated every 15 minutes and volume data of clutter corrected reflectivity factor, mean radial velocity, and spectral width are stored.

Parameter	Value
Low PRF	750 Hz
High PRF	1000 Hz
Unambiguous velocity	39.9 m/s
Maximum range	140 km
Range bin size	0.5 km
Azimuthal speed	24 deg/s
Azimuthal step	1 deg
Number of elevations	10
Elevations (deg)	0.5, 2, 3.5, 5, 7, 9, 12, ...
(De Bilt only)	15, 20, 25

Bilt radar is located at a latitude of 52.10N and a longitude of 5.18E, and the antenna feed is mounted at a height of 44 m above mean sea level. The Den Helder radar is located at a latitude of 52.96N and a longitude of 4.79E, and the antenna feed is mounted at a height of 51 m above mean sea level. The Gematronik radars (Meteor AC360) have an antenna with a 4.2 m diameter and a beam width of about 1 degree. The peak power and width of the transmitted pulses are 250 kW and 0.5 μ s, respectively.

A dedicated Doppler volume scan has been defined on both radars (see table 2.1). This Doppler scan is repeated every 15 minutes and does not interfere with the operational reflectivity scans, which consist of a 4 elevation scan every 5 minutes and a 14 elevation scan every 15 minutes. For each scan the volume data of filtered reflectivity factor, mean radial velocity, and spectral width are stored. Unfortunately, the current radar processing system does not allow for additional storage of the unfiltered reflectivity data. Availability of both the Doppler filtered and unfiltered reflectivity factor volume data would enable a fair comparison with the current ground clutter rejection scheme by Wessels and Beekhuis (1997). The unambiguous velocity range of the Doppler scans is extended using the dual-PRF technique (Sirmans et al., 1976). A discussion on the properties and capabilities of the dual-PRF technique is beyond the scope of this report. An extensive analysis and a technique for correction of dual-PRF velocity data are presented by Holleman and Beekhuis (2003).

The parameters defining the dedicated Doppler scan and corresponding values are displayed in table 2.1. The ratio between the low and high PRF has been set to 3 : 4 in order to extend to unambiguous velocity interval by a factor of 3. The absolute value of the PRFs is a balance between the unambiguous velocity and the maximum range. For wind profiling the maximum

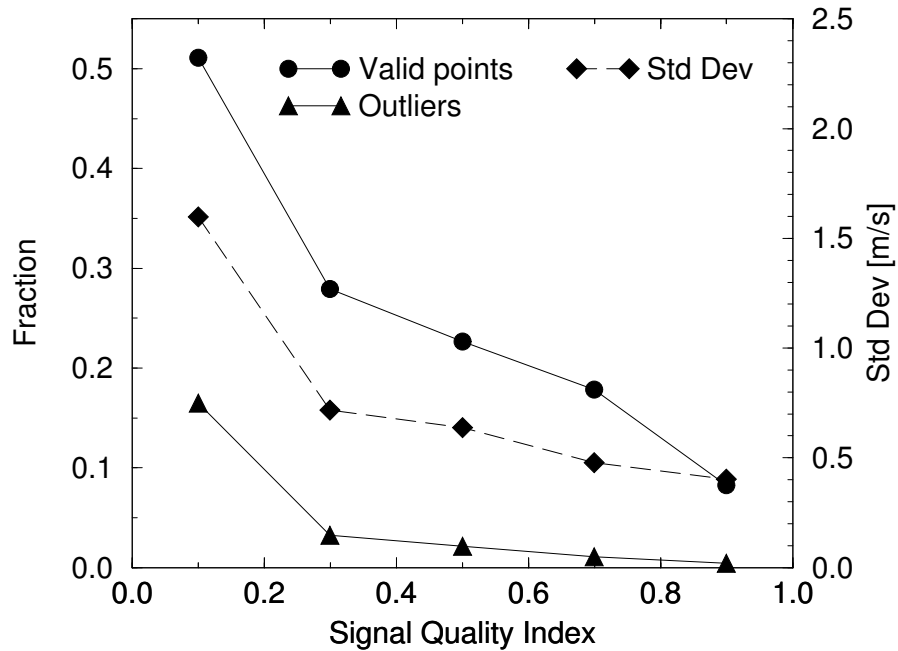


Figure 2.5: The influence of the Signal Quality Index (SQI) threshold on the fraction of valid range bins, the fraction of velocity outliers, and the standard deviation of the velocity estimates. The fraction of outliers is given relative to the number of valid range bins. These data have been collected on 13 September 2001.

range is not an issue, but this Doppler scan strategy has also been used for analyzing the dual-PRF technique (Holleman and Beekhuis, 2003). The range bin size is always a multiple of 0.125 km and its lower limit is determined by the maximum number of range bins that can be processed in real-time (Sigmet, 1998). For a given set of PRFs, the azimuthal speed determines the number of transmitted pulses available for the pulse-pair processing. The azimuthal speed is determined, however, by the available time between the operational reflectivity scans. The 10 elevations have been optimized for profiling up to an altitude of about 6 km. The three highest elevations are not allowed in Den Helder because of regulations from the nearby naval air base.

The default value for Clutter Correction (CCOR) qualifier threshold is -25 dB. To be on the safe side, a CCOR threshold of -20 dB has been selected which will reject somewhat more clutter range bins. For optimizing the Signal Quality Index (SQI), a series of measurements has been performed on 13 September 2001. During the measurement period there were a few scattered showers within range of the radar. The radial velocity data of the lowest elevation of the volume scan data have been analyzed. First of all, the fraction of the number of valid range bins relative to maximum number of bins (100800) has been determined. Then, the velocity of each range bin has been compared with the median of the values in the 3×3 square

Table 2.2: Quality control and filter settings of the RVP6 Doppler signal processor of De Bilt and Den Helder radars for the dedicated Doppler scan.

Parameter	Value
CCOR	-20 dB
SQI	0.5
SIG	0 dB
Filter set	40 dB suppression
Filter number	3

centered on the range bin. Velocities deviating more than 10 m/s from the local median value are counted as outliers and used to calculate the fraction of outliers relative to the number of valid range bins. The other ones are used to calculate the standard deviation of the velocity estimates by summing the squared velocity deviations. In figure 2.5 these “quality estimators” have been plotted as a function of the applied Signal Quality Index. It is evident that the SQI thresholding has an influence on both the number of valid range bins and the mean quality of the velocity estimates, i.e., the number of outliers and the standard deviation. The SQI qualifier threshold has been set to 0.5, which is also the default value. Finally, the Weather Signal Power (SIG) qualifier threshold, which is only relevant for spectral width data, has been set to its lowest value (0 dB). In this way spectral width information will be available for all range bins containing valid mean velocity information.

The RVP6 Doppler signal processor offers two sets of Infinite Impulse Response filters for ground clutter suppression by digital time domain filtering. One set for 40 dB suppression of ground clutter and one set for 50 dB suppression (Sigmet, 1998). A series of measurements has been performed in order to select the appropriate IIR filter. These measurements have been performed on 13 September 2001, on the same day and under the same circumstances as the previous SQI measurements. For each 40 dB suppression filter, an azimuthal Doppler scan at 0.5 degrees elevation has been performed. The 50 dB suppression filters will not be used, because they remove a larger part of the Doppler spectrum (see section 2.4). The Doppler scans are used to generate histograms of the mean radial velocity by counting for each velocity interval the number of range bins. In figure 2.6 the obtained histograms are shown for the unfiltered scan (Filter 0) and the seven filtered scans (Filter 1 – 7). The filter functions of the seven filters are shown in figure 2.4 where filter 1 is the narrowest filter and filter 7 the widest. The histogram of the unfiltered Doppler scan shows a clear peak at zero mean velocity due to ground clutter. When increasingly wider filters are applied, the peak at zero velocity gradually disappears and an increasingly deeper hole is burned in the Doppler spectrum. It is evident from figure 2.6 that a balance between residual ground clutter and loss of hydrometeor signal has to be found. Based on this figure, IIR filter 3 with a 40 dB suppression of ground clutter

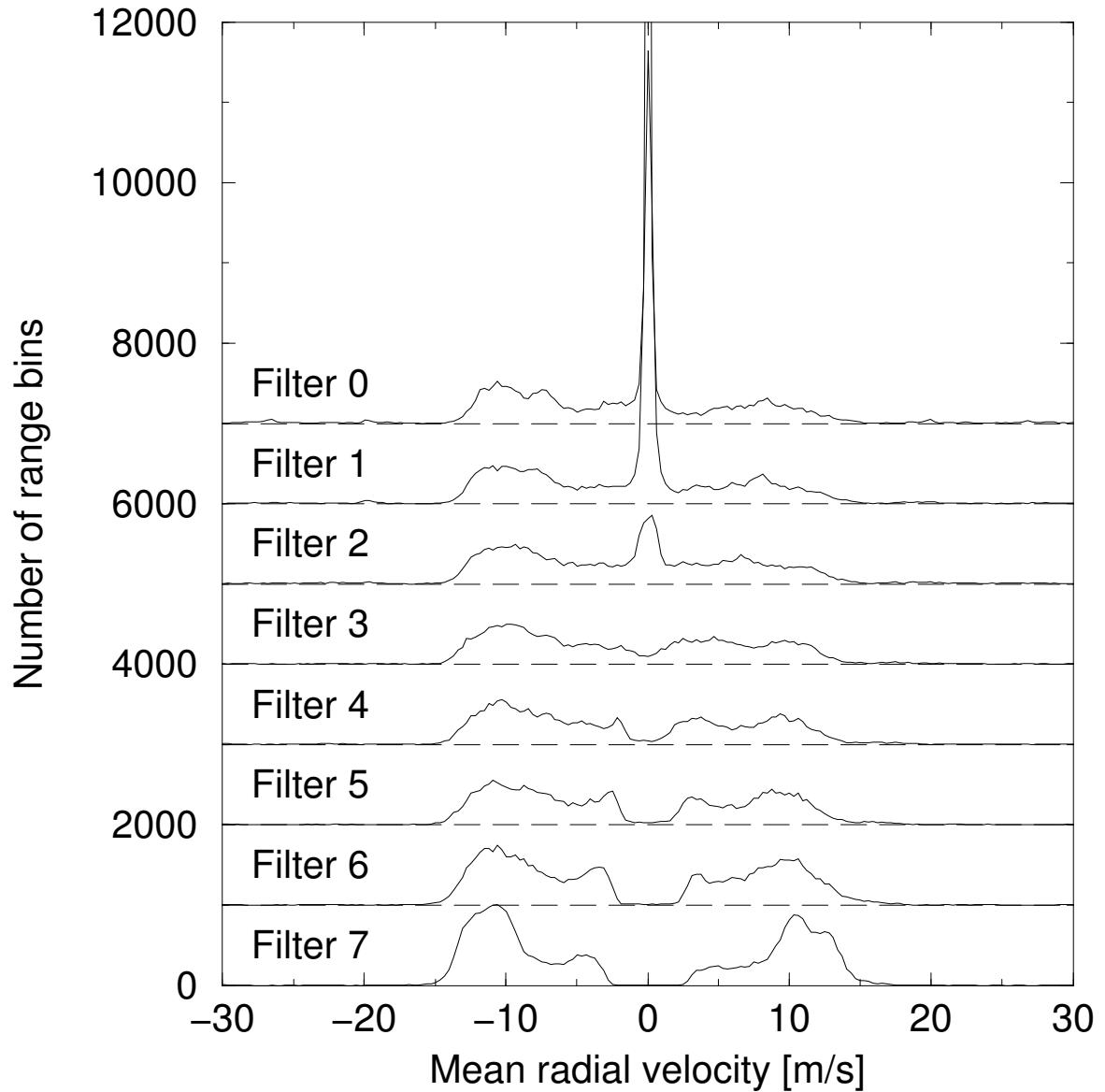


Figure 2.6: This figure shows the influence of the IIR filter setting on the amount of ground clutter. Each curve represents an histogram of the observed mean radial velocities within a scan at 0.5 degrees elevation. Only IIR filters with a suppression of 40 dB are listed. These data have been collected on 13 September 2001.

has been selected for the KNMI Doppler radars. The quality control and filter settings of the RVP6 Doppler signal processor have been summarized in table 2.2.

Chapter 3

Methods for Wind Profile Retrieval

3.1 Radial Velocity from Local Wind Model

A Doppler weather radar measures the radial component of the velocity of scattering hydrometeors. To be able to extract information on the local wind field, one has to assume that the velocity vector of the observed scatterers is equal to the local wind vector. It will be detailed below that this important assumption is not always valid. The Doppler weather radar performs a three-dimensional scan and thus provides the mean radial velocity as a function of range, azimuth, and elevation. In the case of single-Doppler radar wind profile retrieval, information on the local wind field has to be deduced from these radial velocity volume data only. A schematic overview of the typical Doppler radar geometry and the relevant local wind field vectors is presented in figure 3.1. The figure shows clearly the three scanning directions of a (Doppler) weather radar and the three components of the local wind field: the radial velocity V_r , the tangential velocity V_t , and the vertical velocity w . Because only one of these components V_r can be observed by the Doppler radar, the other two components of the wind field have to be estimated using a local wind model.

For wind profiling by single-Doppler radar a linear wind model is usually taken to approximate the wind field in the vicinity of the radar. This linear wind model is centered horizontally at location of the radar and vertically at the height of interest z_0 . The components of the local wind field in the x -, y -, and z -directions are $U(\vec{r})$, $V(\vec{r})$, and $W(\vec{r})$, respectively, and in the linear wind model they are approximated by:

$$U(\vec{r}) = u_0 + x \frac{\partial u}{\partial x} + y \frac{\partial u}{\partial y} + (z - z_0) \frac{\partial u}{\partial z} \quad (3.1)$$

$$V(\vec{r}) = v_0 + x \frac{\partial v}{\partial x} + y \frac{\partial v}{\partial y} + (z - z_0) \frac{\partial v}{\partial z} \quad (3.2)$$

$$W(\vec{r}) = w_0 + (z - z_0) \frac{\partial w}{\partial z} \quad (3.3)$$

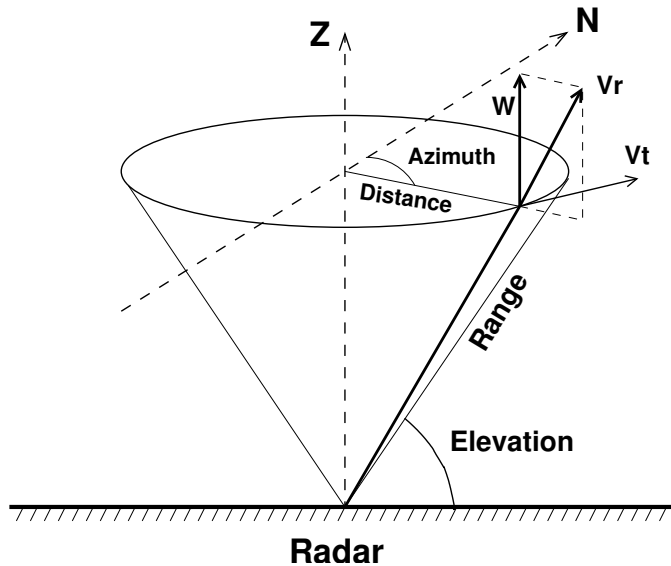


Figure 3.1: Schematic overview of the radar geometry used to measure Doppler wind profiles. The range, azimuth, and elevation, which are the scanning directions of a weather radar, are indicated. In addition, the radial velocity V_r , the tangential velocity V_t , and the vertical velocity w components of the local wind field are shown.

where u_0 , v_0 , and w_0 are the components of the wind field in the center and $\partial u / \partial x$ (and similar terms) are partial derivatives of the wind field at the center. Waldteufel and Corbin (1979) have shown that the partial derivatives of W in the x - and y -directions enter the equation for the radial velocity only in combination with the partial derivatives of U and V in the z -direction. In locally stratiform situations, where the linear wind model is most likely to apply, the horizontal derivatives of the vertical velocity are much smaller than the vertical derivatives of the horizontal velocities, and they can, therefore, be neglected (Waldteufel and Corbin, 1979). The other partial derivatives of the linear wind model represent divergence and deformation of the local wind field (Browning and Wexler, 1968):

$$\frac{\partial u}{\partial x} + \frac{\partial v}{\partial y} : \text{ Divergence } (\hat{D}) \quad (3.4)$$

$$\frac{\partial u}{\partial x} - \frac{\partial v}{\partial y} : \text{ Stretching deformation } (\hat{T}) \quad (3.5)$$

$$\frac{\partial u}{\partial y} + \frac{\partial v}{\partial x} : \text{ Shearing deformation } (\hat{H}) \quad (3.6)$$

In particular the extraction of the divergence from Doppler radar observations has gained much attention in recent years (Browning and Wexler, 1968; Matejka and Srivastava, 1991; Cifelli et al., 1996)

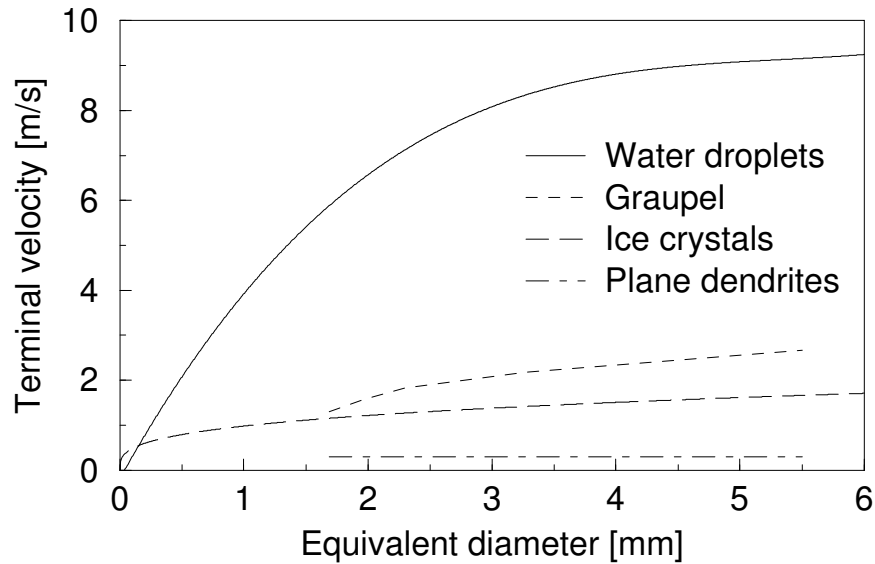


Figure 3.2: Terminal fall velocity of water droplets and ice crystals as a function of the equivalent diameter, i.e., the diameter of the water sphere with the same mass. These curves are generated using data from Foote and DuToit (1969) for water droplets, from WMO (1966) for graupel and plane dendrites, and from Gunn and Marshall (1958) for ice crystals.

In addition to their motion due to the local wind field, the hydrometeor scatterers have a terminal fall velocity. The terminal fall velocity is denoted as W_f and is negative because the z -axis is pointing upwards. In figure 3.2 the terminal fall velocity of water droplets and several kinds of solid precipitation is plotted as function of the equivalent diameter, which is the diameter of the water sphere with the same mass. It is evident that the terminal velocity of hydrometeors below the melting layer can be substantial, i.e., up to 9 m/s, and thus it is usually larger than the vertical component of the local wind field. The extraction of horizontal wind field parameters (u_0 and v_0) can be troubled by inhomogeneity of the terminal velocity of hydrometeors within the analysis volume (Browning and Wexler, 1968). Doppler radar observations above the melting layer there is less of a problem due to the much lower terminal fall velocity of ice crystals. Localized convection and corresponding (strong) updrafts can also interfere with the extraction of the horizontal wind field parameters. In cases with strong updrafts the wind field extraction will usually be unsuccessful.

The modeled radial velocity at a certain position can be calculated from the linear wind model and the terminal fall velocity of the hydrometeors. The radial velocity at (x,y,z) due to the local wind field is the component of the field along the line of sight of the radar, i.e., the line connecting the origin and point (x,y,z) . The radial velocity is the sum of the terminal fall

velocity and the scalar product of the wind field vector and the line-of-sight vector:

$$V_r = \frac{x}{R} \cdot U(\vec{r}) + \frac{y}{R} \cdot V(\vec{r}) + \frac{z}{R} \cdot (W(\vec{r}) + W_f) \quad (3.7)$$

$$= \sin \phi \cos \theta U(\vec{r}) + \cos \phi \cos \theta V(\vec{r}) + \sin \theta (W(\vec{r}) + W_f) \quad (3.8)$$

where $R \equiv |\vec{r}|$ is the range from the radar, and ϕ and θ are the azimuth and elevation of the radar beam. Assuming a uniform wind field, i.e., all partial derivatives in equations 3.1-3.3 are neglected, the most elementary equation for the radial velocity is obtained:

$$V_r^{(1)} = (w_0 + W_f) \sin \theta + u_0 \cos \theta \sin \phi + v_0 \cos \theta \cos \phi \quad (3.9)$$

The next level of complexity of the radial velocity equation is obtained by only neglecting the vertical partial derivatives in the equations for the linear wind model. This gives rise to three higher-order terms in the radial velocity equation:

$$V_r^{(2)} = V_r^{(1)} + \frac{\hat{D}}{2} R \cos^2 \theta + \frac{\hat{H}}{2} R \cos^2 \theta \sin 2\phi + \frac{\hat{T}}{2} R \cos^2 \theta \cos 2\phi \quad (3.10)$$

The divergence \hat{D} , the shearing deformation \hat{H} , and stretching deformation \hat{T} of the horizontal wind field have been defined previously. The most comprehensive form of the radial velocity equation is obtained by using the full linear wind model:

$$V_r^{(3)} = V_r^{(2)} + \frac{\partial w}{\partial z} \Delta z \sin \theta + \frac{\partial u}{\partial z} \Delta z \sin \theta \sin \phi + \frac{\partial v}{\partial z} \Delta z \sin \theta \cos \phi \quad (3.11)$$

where $\Delta z = R \sin \theta - z_0$ is the deviation from the height of interest. The preceding three equations describe the radial velocity as deduced from a local wind model with an increasing level of complexity. These equations will (partly) be used for the wind profiling methods described below.

3.2 Velocity Azimuth Display

Lhermitte and Atlas (1961), and Browning and Wexler (1968) have developed the Velocity Azimuth Display (VAD) retrieval method in the sixties. When the mean radial velocity at constant range and elevation is displayed as a function of azimuth, the resulting curve will have the form of a sine, see equation 3.9. The wind speed and direction can be determined from the amplitude and the phase of this sine, respectively. Figure 3.3 shows an example of a VAD recorded on 20 January 2003 around 18:54 UTC. This VAD is taken at an elevation of 12 degrees and a range of 7.5 km, and it clearly shows the expected sine. The deduced maximum wind speed and wind direction are 20.4 m/s and 217 degrees, respectively. In other words, a wind of 40 knots is blowing from the southwest at an altitude of 1.5 km.

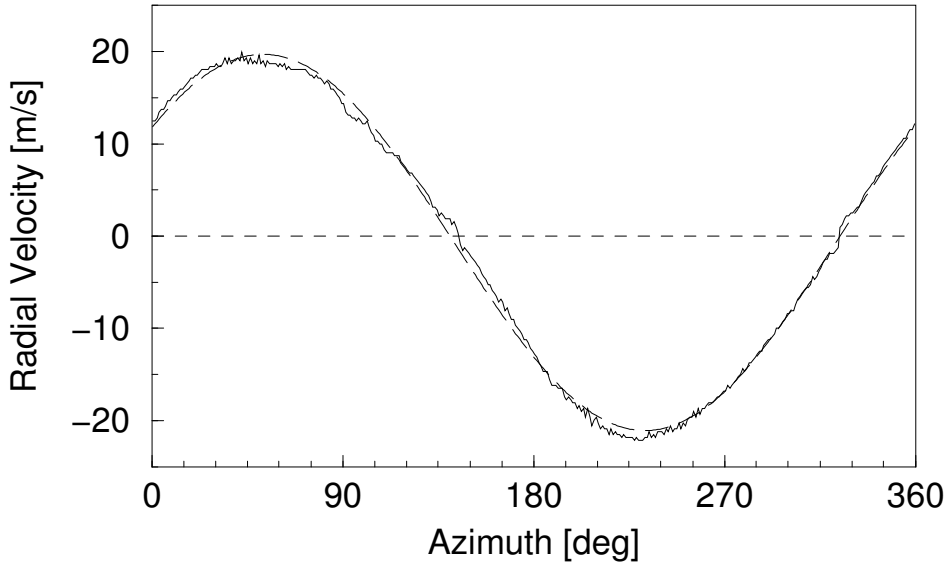


Figure 3.3: Example of a Velocity Azimuth Display (VAD) obtained from a volume measurement from 18:54 UTC on 20 January 2003. These data have been recorded at an elevation of 12 degrees and a range of 7.5 km. The long-dashed curve shows a sine fit through the observed VAD.

The quantitative analysis of an observed VAD is usually done via a Fourier series decomposition. The radial velocity as a function of the azimuth is modeled by a truncated Fourier series:

$$V_r(\phi) = \frac{a_0}{2} + \sum_{n=1}^N a_n \cos n\phi + \sum_{n=1}^N b_n \sin n\phi \quad (3.12)$$

The Fourier coefficients a_n and b_n are determined by a fit of this series to the observed VAD. It has been suggested that the VAD retrieval methods is more robust than other methods (see below) because the fitting basis functions used in the VAD analysis are orthogonal and independent of the local wind model (Srivastava et al., 1986). The orthogonality of the basis functions is reduced, however, by presence of gaps in the collected data (Matejka and Srivastava, 1991). In addition, the obtained Fourier coefficients can only be interpreted using a local wind model. Two different models for the interpretation of the Fourier coefficients are distinguished in this study.

VAD1: Assuming a uniform local wind and thus using the most elementary equation for the radial velocity (equation 3.9), the three lowest Fourier coefficients are interpreted as:

$$a_0 = 2 \sin \theta (w_0 + W_f) \quad (3.13)$$

$$a_1 = \cos \theta v_0 \quad (3.14)$$

$$b_1 = \cos \theta u_0 \quad (3.15)$$

and all other coefficients are expected to be negligible.

VAD2: When only the vertical partial derivatives in the linear wind model are neglected (see equation 3.10), a more frequently used interpretation of the five lowest Fourier coefficients is obtained:

$$a_0 = 2 \sin \theta (w_0 + W_f) + R \cos^2 \theta \hat{D} \quad (3.16)$$

$$a_1 = \cos \theta v_0 \quad (3.17)$$

$$a_2 = R \cos^2 \theta \hat{T}/2 \quad (3.18)$$

$$b_1 = \cos \theta u_0 \quad (3.19)$$

$$b_2 = R \cos^2 \theta \hat{H}/2 \quad (3.20)$$

and again all other coefficients are expected to be negligible.

Because the basis functions of the VAD analysis are (almost) orthogonal, there should not be any difference in the wind field parameters (u_0, v_0) extracted using a Fourier series decomposition onto three basis functions or onto five functions. The divergence of the horizontal wind field \hat{D} appearing in Fourier coefficient a_0 has gained a lot of interest. Unfortunately it appears in combination with the vertical velocity and the terminal fall velocity. Matejka and Srivastava (1991) have proposed an Extended Velocity Azimuth Display (EVAD) analysis which employs a series of VADs at different elevations to separate the contributions of the vertical velocities and the divergence to the first Fourier coefficient.

3.3 Volume Velocity Processing

One disadvantage of the VAD retrieval method is that the conversion of a Doppler volume scan to a wind profile is not straightforward. For each height layer, several VADs are usually available which all have to be quality controlled and fitted to obtain a set of wind field parameters (u_0, v_0) . The sets of wind field parameters have to be combined to a final set which is representative for the height layer of interest, which is usually done by a weighted average (Matejka and Srivastava, 1991). In table 3.1 the calculated number of VADs and number of range bins available per height layer of 200 m thickness are presented. These numbers have been calculated based on the scan strategy parameters given in table 2.1. It is evident that, especially at low altitudes, many VADs per height layer are available for determining the local wind field. Instead of processing a series of VADs, it makes more sense to process all available Doppler volume data within a height layer at once. Waldteufel and Corbin (1979) have introduced the so-called Volume Velocity Processing (VVP) retrieval method.

Table 3.1: This table shows the number of VADs and the number of range bins available for each height layer (200 m thick). The numbers have been calculated based on the scan strategy described in table 2.1

Height [km]	Number of VADs	Number of range bins
5.9	3	1080
5.7	3	1080
5.5	3	1080
5.3	6	2160
5.1	5	1800
4.9	6	2160
4.7	5	1800
4.5	6	2160
4.3	6	2160
4.1	6	2160
3.9	7	2520
3.7	8	2880
3.5	9	3240
3.3	7	2520
3.1	11	3960
2.9	11	3960
2.7	12	4320
2.5	11	3960
2.3	13	4680
2.1	14	5040
1.9	15	5400
1.7	16	5760
1.5	18	6480
1.3	19	6840
1.1	19	6840
0.9	23	8280
0.7	25	9000
0.5	22	7920
0.3	20	7200
0.1	37	13320

The Volume Velocity Processing method extracts the parameters of the local wind field by a multi-dimensional linear fit of the radial velocity equation to the observed Doppler volume data. The equations for the radial velocity given previously, equations 3.9-3.11, suggest three different VVP algorithms with an increasing level of complexity:

VVP1: VVP algorithm based on the most primitive equation for the radial velocity (3.9). In this case the radial velocity is a function of azimuth ϕ and elevation θ , and only three wind field parameters are fitted: u_0 , v_0 , and $(w_0 + W_f)$.

VVP2: In this case equation 3.10 for the radial velocity is used which in addition depends on the range from the radar R . Apart from the three wind field parameters listed above, three parameters containing information on the horizontal derivatives of the local wind field, i.e., \hat{D} , \hat{H} , and \hat{T} , are fitted.

VVP3: The most comprehensive VVP algorithm uses equation 3.11 for the radial velocity which also includes the vertical derivatives of the local wind field: $\partial u / \partial z$, $\partial v / \partial z$, and $\partial w / \partial z$. In this algorithm, the local wind field is described by 9 parameters and the radial velocity is a function of azimuth, elevation, range, and height of interest z_0 .

In their original article Waldteufel and Corbin (1979) proposed the most comprehensive implementation of the VVP method, because knowledge of the vertical derivatives allows in principle for a quality control of the extracted parameters by comparison of successive height layers. Boccippio (1995) argues that the vertical derivatives should be discarded to avoid problems with linear dependencies between different basis functions, and he favors the use of the VVP2 retrieval technique.

It has been a matter of debate whether or not the VVP method for retrieval of wind profiles is as robust as the VAD method, because the VVP basis functions are not inherently orthogonal. It has already been mentioned, however, that the orthogonality of the VAD basis functions is reduced by the presence of gaps in the collected data (Matejka and Srivastava, 1991). Boccippio (1995) presents an extensive diagnostic analysis of the VVP retrieval method and he concludes that a relatively simple subset (VVP2) of the original 11-parameter model can be used to obtain a robust and stable fit. This is corroborated by the observation that several commercial manufacturers, like Gematronik GmbH and Sigmet Inc., offer VVP modules for operational implementation.

3.4 Sources of Error

In this section several sources of error which can affect the quality of the Doppler radar wind profiles are discussed. In addition, possible ways to reduce problems caused by these potential sources of error are discussed.

A Doppler radar can only determine the mean radial velocity when a scattered signal is received. The absence of hydrometeors or other scatterers leads to gaps or “no data” regions in the radial velocity data. Wind profile retrieval methods have problems with large regions of no data, because the basis functions loose orthogonality and/or the linear fit becomes unstable. To avoid gross errors, no wind field retrieval should be performed on Doppler volume data with large gaps. The VVP retrieval may theoretically be stable up to sector gaps of 60-90 degrees, but extreme caution has to be taken in such cases (Boccippio, 1995).

It has been detailed in section 2.6 that the unambiguous interval of the mean radial velocity is extended by a factor of 3 using the dual-PRF technique (Sirmans et al., 1976). Analysis of dual-PRF velocity data has revealed that a small fraction of the range bins will always be dealiased incorrectly (Holleman and Beekhuis, 2003). These velocity outliers constitute typically 1 percent of the range bins, and the velocity error will be twice the low or high unambiguous velocity of the primary observations, i.e., 20 or 26 m/s in our case. The outliers can efficiently be detected by a comparison with the modeled radial velocity obtained from a first fit. After removal of the outliers, the final values for the wind field parameters can be retrieved from a second fit.

Possible ground clutter in the received Doppler signal is suppressed using a digital time or frequency domain filter before the mean radial velocity is calculated (see section 2.4). Strong ground clutter is not suppressed completely, however, and it will cause a bias of the mean radial velocity towards zero. In the absence of hydrometeor echoes this error is frequently evident from an apparent wind speed which is close to zero. This error can effectively be avoided by removal of all mean radial velocities close to zero (< 2 m/s) before the wind profile retrieval method is applied. For significant wind speeds this will hardly have an effect, but wind speeds close to zero, true or false, will never be retrieved.

The variability of the terminal fall velocity of the hydrometeors within the analysis volume, with an estimated maximum of 4 m/s for water droplets and 1 m/s for ice crystals (Browning and Wexler, 1968), can cause errors in the retrieved horizontal winds. From equation 3.9, it can be seen that the coupling between the hydrometeor velocity W_f and the horizontal wind parameters depends on the elevation used. The error due to variability of the terminal fall velocity can, therefore, be minimized by limiting the elevation. For wind field retrieval below the melting layer, Browning and Wexler (1968) suggest a maximum elevation of 9 degrees.

The retrieval methods for wind profiles approximate the local wind field by a uniform or a linear wind model. Inevitably deviations of the local wind field from the wind model will cause errors in the retrieved wind parameters. Caya and Zawadzki (1992) have investigated the effect of nonlinearity of the local wind field on the quality of the VAD retrieval. They have derived a new interpretation of the five lowest Fourier coefficients by assuming a horizontal wind field with a cubic spatial dependence. It is concluded that the parameters of the VAD analysis have no clear physical meaning when the wind field is nonlinear. The value a_1 and b_1 represent neither the mean wind within the VAD circle nor the wind at the radar site. Intuitively it is expected that for weak nonlinearities the associated errors should be small (Caya and

Table 3.2: Overview of the default parameters used to calculate and quality control the Doppler radar wind profiles. The meaning of all parameters is described in the text. Note that a “Number of standard deviations” equal to zero implies a fixed threshold given by the “Velocity deviation threshold”.

Parameter	Default value
Height of antenna feed	0.05 km
Layer thickness	0.20 km
Number of layers	30
Minimum range	5.0 km
Maximum range	25.0 km
Maximum height	2.0 km
Maximum elevation	9.5 deg
Minimum radial velocity	2.0 m/s
Number of sectors	8
Number of points per sector	5
Velocity deviation threshold	10.0 m/s
Number of std.dev.	0 (not used)

Zawadzki, 1992). Errors due to nonlinearities of the wind field are reduced by limiting the diameter of the retrieval volume.

Non-hydrometeor scatterers such as insects and birds are detected by Doppler radar as well. While some insects can provide a help in defining the boundary layer wind (Wilson et al., 1994; Riley, 1999), migrating birds and actively flying insects are a major source of error for wind profile retrieval methods (Koistinen, 2000; Collins, 2001). Bird migration can be recognized by inconsistency of the wind vectors or by deviation of the Doppler wind profiles from reference profiles. In spring erroneous northerly winds will appear, while in autumn erroneous southerly winds will be seen. The problem of bird migration will be discussed in more detail in section 5.5.

3.5 Implementation

A C-program has been written that reads a file with radial velocity volume data and calculates a wind profile using the VAD1, VAD2, VVP1, VVP2, or VVP3 retrieval method. The wind profile is calculated layer by layer, and by default the layer thickness and the number of layers are set to 0.2 km and 30, respectively.

The available radial velocity data within the height layer of interest are collected and quality controlled. Only velocity data from range bins between a minimum and maximum range from

the radar are taken into account. Absolute radial velocities under 2.0 m/s (default) are ignored. Beneath a certain height which should be related to the actual melting layer height, only velocity data below a maximum elevation will be used. For simplicity a fixed melting layer height of 2.0 km is used in this study. The azimuthal circle is divided into a number of sectors and for each sector the number of collected velocity data points is counted. When the number of points in two neighboring sectors are below a certain number, a sector gap is detected and the height layer will not be processed any further.

The collected radial velocity data are matched to the appropriate model equation using a general linear least squares method. The most straightforward way to obtain a solution for a general linear least squares problem is based on normal equations. The solution using normal equations is susceptible to roundoff errors. In addition, the normal equations are often almost singular and then no solution is found at all. The cure for these problems is a solution by Singular Value Decomposition (SVD) which gives the best approximation in least-squares sense (Press et al., 1992). For the VAD retrieval methods, the Fourier coefficients are determined from SVD solution for each individual VAD within the height layer of interest. The wind field parameters, which are extracted from the Fourier coefficients, are weighted by the number of points and averaged over all VADs within the height layer. For the VVP retrieval methods, the wind field parameters are determined from a single SVD solution for all available data within the height layer of interest. The standard deviation of the radial velocity σ is calculated from the SVD solution using the chi-square merit function (Press et al., 1992):

$$\sigma^2 = \sum_{i=1}^N (V_{r,i} - V_r(\vec{r}_i))^2 / (N - M) \quad (3.21)$$

where N is the number of radial velocity data and M is the number of parameters in the radial velocity model. After a first fit, velocity outliers due to dealiasing errors are traced by comparing the observed radial velocity $V_{r,i}$ with the modeled radial velocity $V_r(\vec{r}_i)$. When the deviation is more than a threshold value, the observed radial velocity is removed from the data. This threshold value can be either a multiple of the standard deviation of the radial velocity or a fixed value. After removal of the outliers, the data collection and quality control are repeated and the final wind field parameters are again determined from (multiple) SVD solution(s).

To obtain a wind profile, the wind parameter retrieval is repeated for all height layers within the profile. For each successful retrieval, the following (wind field) parameters are stored for further analysis:

- Horizontal wind field parameters: u_0 and v_0 , which can easily be converted to wind speed ff and wind direction dd
- Sum of the vertical wind velocity and the terminal fall velocity of the hydrometeors: $w_0 + W_f$
- Standard deviation of the radial velocity as determined from the SVD solution using the chi-square merit function: σ

- Variance of the retrieved wind field parameters as deduced from the SVD solution
- Number of radial velocity data that has contributed to the wind parameter retrieval: N

In addition to the wind profiles, corresponding profiles of reflectivity factor Z and Doppler spectral width W are constructed by calculating for each height layer the median of the available data.

Chapter 4

Intercomparison of Wind Profile Retrieval Techniques

4.1 Available Wind Profile Data

Wind profile data have been collected over a period starting 1 October 2001 and ending 30 June 2002. During this 9 month period (wind profile) data from the Doppler radars, from the radiosondes, and from the Hirlam Numerical Weather Prediction (NWP) model have been gathered. The scan strategy of the Doppler radars (see section 2.6) was finalized by the end of September 2001, and this sets the starting date of the verification period. The ending date is determined by the temporary termination of the radiosonde launches at De Bilt on 1 July 2002. The radiosonde launching at De Bilt was resumed in November 2002, but the number of launches per day was reduced from 4 times a day to twice a day.

For the Doppler radar in De Bilt both Doppler volume scan data and processed wind profiles have been collected, and for Den Helder only processed wind profiles have been collected. 22610 Different wind profiles/volume scans have been collected over the given period. The available volume scan data contain 3-dimensional reflectivity factor, mean radial velocity, and spectral width information. At both radar sites wind profiles are calculated from the mean radial velocity data using the Rainbow VVP module (Gematronik, 2003), which will be referred to as R-VVP3 in the remaining. This commercial implementation of the Volume Velocity Processing retrieval method was delivered with the KNMI Doppler radars. The settings of the R-VVP3 module are in agreement with the default parameters of the implemented wind profiling retrieval methods (see table 3.2).

During the verification period Vaisala RS90-AL radiosondes were launched 4 times a day at De Bilt. Temperature, humidity, wind speed, and wind direction profiles with a vertical resolution of 60-70 m are obtained. The radiosonde profiles are binned into 200 m thick height layers in order to facilitate comparison with the Doppler radar profiles. The Cartesian horizontal components of the wind vectors were averaged in the height bins. The radiosonde profiles

Table 4.1: Overview of available (wind) profile information in this study. The source is either Doppler radar, radiosonde , or Hirlam. Wind profiles are retrieved from volume scan data by the retrieval methods described previously. The number of available profiles per day is given in the last column.

Source	Data	Location	Number
Doppler radar	Volume scans	De Bilt	96
	Rainbow wind profiles	De Bilt	96
	Rainbow wind profiles	Den Helder	96
Radiosonde	Profiles	De Bilt	4
Hirlam NWP	Profiles	De Bilt	8
	Profiles	Den Helder	8

are always assigned to the main hours, but radiosondes are typically launched 30 minutes before the main hours. Because the weather radar only provides wind vector data in the lower part of the troposphere, the radiosonde wind profiles will be compared with weather radar profiles observed 30 minutes before the main hours.

The High Resolution Limited Area Model (Hirlam) which is being developed by a consortium of 8 European countries (Unden et al., 2002) is run operationally at KNMI. The model analyzes the state of the atmosphere 8 times a day, and it makes 48-hour forecasts only 4 times a day. During the verification period, the hydrostatic Hirlam model used 31 vertical levels and a horizontal resolution of 55 km (22 km from 5 March 2002). Profiles of temperature, mixing ratio, and the model-grid aligned horizontal wind field components have been extracted from the model's initialized analysis at the grid points nearest to De Bilt (distance 11 km) and Den Helder (distance 15 km). The pressures at the vertical levels have been converted to geometric heights by integration of the hydrostatic equation using temperature and mixing ratio information. The model-grid aligned wind components have been rotated to obtain true northerly and easterly wind field components. In addition, the profiles have been interpolated to a 200 m height layer spacing to facilitate comparison with radar wind profiles. The Hirlam profiles at De Bilt will be correlated to the radiosonde profiles because these profiles are assimilated in the model.

4.2 Doppler Wind Profiles against Radiosonde

The Doppler radar wind profiles at De Bilt have been verified against the profiles from the collocated radiosonde station. For this, pairs of wind vectors from the radar and radiosonde with matching time and height coordinates are collected. This collection of wind vector pairs and the associated information is used to calculate a number of verification parameters, like the

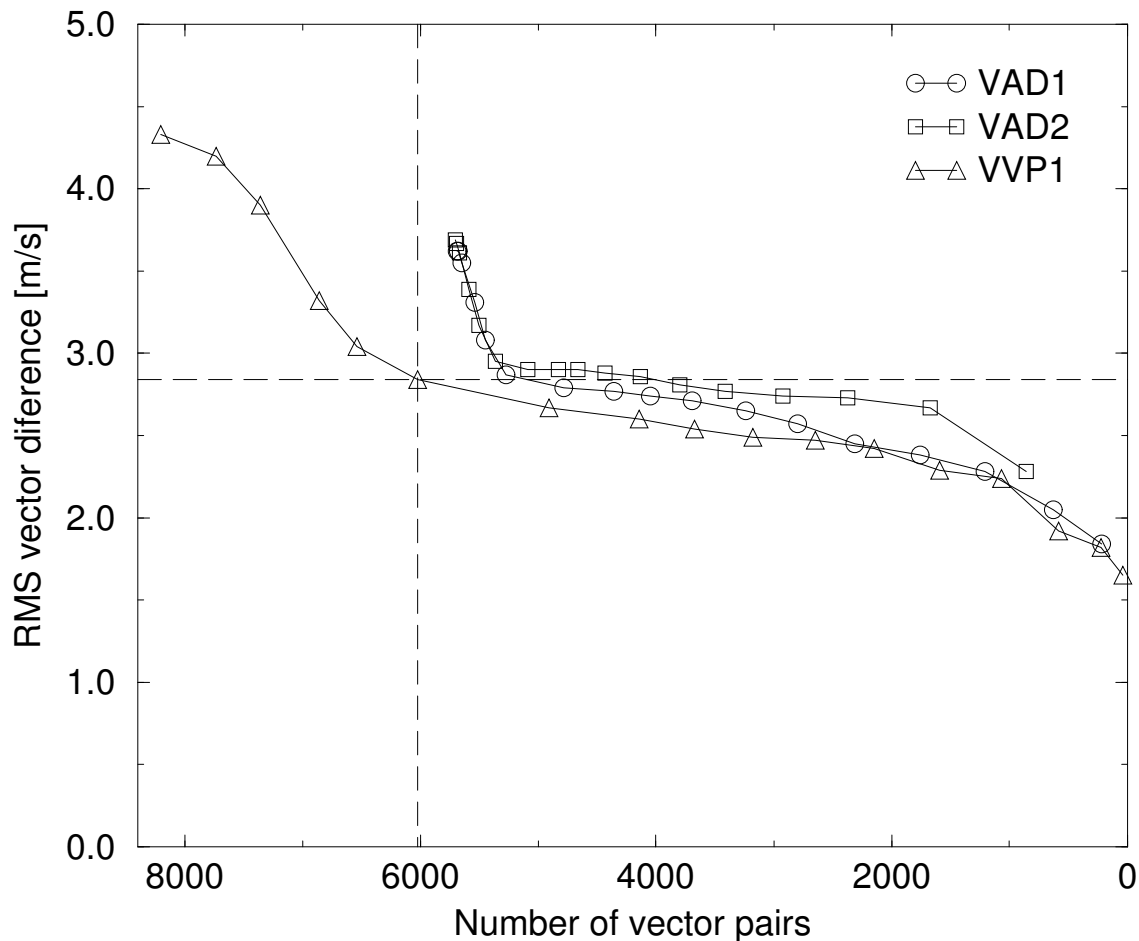


Figure 4.1: The rms vector differences between radar and radiosonde wind vectors as a function of the number of vector pairs. The number of wind vector pairs is changed via a selection on the standard deviation of the radial velocity σ . Curves for two Velocity Azimuth Display (VAD) methods and one Volume Velocity Processing (VVP) method are shown. The dashed cross marks the suggested threshold for the VVP1 wind vectors (see text).

root-mean square (rms) vector differences, the bias and standard deviation of wind speed, wind direction, and Cartesian components.

In figure 4.1 the rms vector differences is plotted as a function of the number of wind vector pairs for three different wind profile retrieval methods. The number of wind vector pairs is varied by changing the threshold on the allowed standard deviation. The standard deviation of the radial velocity σ is determined for each wind vector during the wind profile retrieval and it is a direct measure for the quality of the wind vector retrieval (see section 3.5). The three wind profile retrieval methods are labeled according to the convention introduced in chapter 3. The rms vector differences vary from roughly 1.5 to 4.5 m/s, and the number of wind vector pairs ranges from zero to about 8000. Figure 4.1 shows two important aspects of the wind profile retrieval methods: quality and availability. Retrieval methods that combine high quality, i.e., a low rms vector differences, with a high availability, i.e., large number of wind vector pairs, are preferred. It is evident from the figure that the VVP1 retrieval method performs much better than the two VAD methods. This is mainly due to the lower availability of the VAD wind vectors. During VAD retrieval all velocity azimuth display circles are quality controlled individually, while during VVP retrieval all velocity data within a height layer are quality controlled collectively. A sector gap and thus a rejection from further processing will, therefore, be more likely for the VAD than for the VVP retrieval.

For the other VVP retrieval methods, the rms vector differences as a function of the number of wind vector pairs is shown in figure 4.2. The corresponding curve for the VVP1 retrieval method is plotted again to facilitate comparison. Currently the Rainbow VVP module (Gematronik, 2003) does not provide information on the standard deviation of the radial velocity, and therefore the wind vectors cannot be selected based on this criterion. It is evident from the figure that the performance of the VVP retrieval methods is rather similar, but VVP1 performs slightly better than the other retrieval methods. It has been detailed in section 3.3 that the complexity of the wind model used in the VVP retrieval method increases with the method's number (1-3). The verification results for the horizontal wind vectors presented in figure 4.2 suggest that the retrieval based on the most simple wind model provides the best horizontal wind data. This important result may be counterintuitive, but it is most likely due to the non-orthogonality of the VVP basis functions. The addition of the higher-order basis functions with (small) linear dependencies can degenerate the robustness of the regression method and cause fluctuations of the retrieved wind field parameters (Boccippio, 1995). The performance of the Rainbow VVP module (R-VVP3) is substantially worse than the VVP1-3 implementations which is probably due to the use of normal equation regression instead of SVD (see section 3.5) and to application of the standard deviation threshold in between the two wind model fits instead of after the second fit.

The actual choice for the threshold on the allowed standard deviation has to balance the quality of the wind vectors with their availability. The shape of the rms vector differences versus number of wind vectors curves naturally suggest a threshold just below the bending point where the difference vector is about 2.8 m/s and the number of vectors is around 6000.

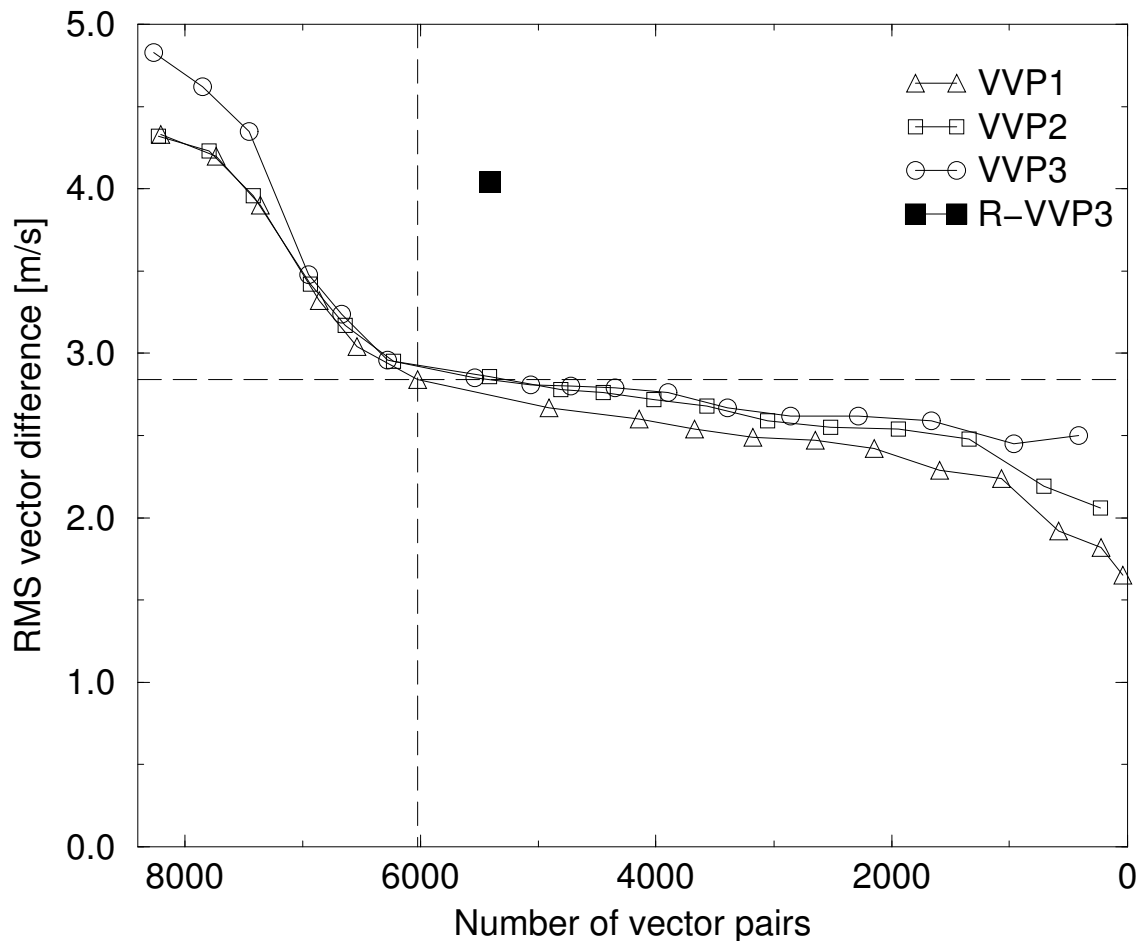


Figure 4.2: The rms vector differences between radar and radiosonde wind vectors as a function of the number of vector pairs. The number of wind vector pairs is changed via a selection on the standard deviation of the radial velocity. Curves for the three implemented Volume Velocity Processing (VVP1-3) methods and the Rainbow VVP module (R-VVP3) are shown. The dashed cross marks the suggested threshold for the VVP1 wind vectors.

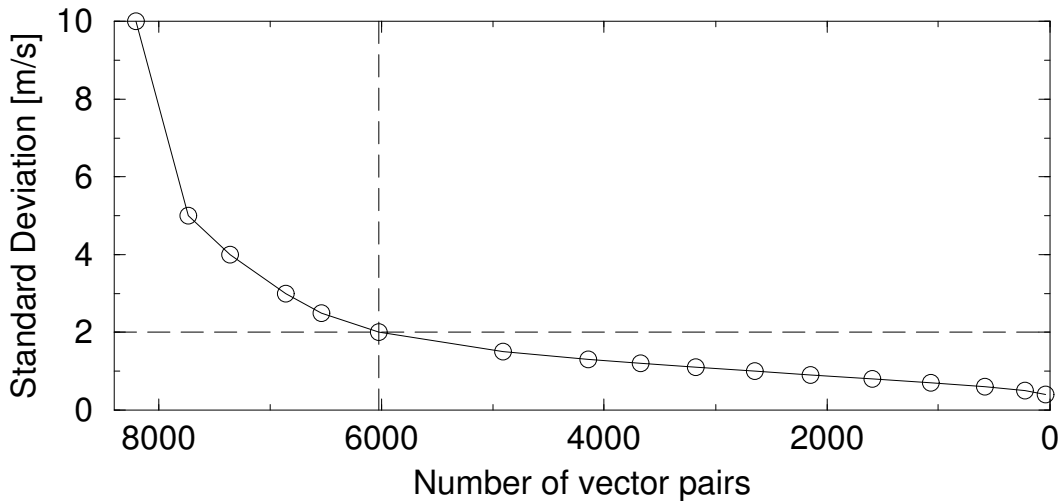


Figure 4.3: This figure shows the threshold on the allowed standard deviation versus the number of available wind vectors for the VVP1 retrieval method. This figure can be used to translate a number of vector pairs in figures 4.1 and 4.2 into the applied standard deviation threshold. The dashed cross marks the suggested standard deviation threshold for the VVP1 wind vectors.

The dashed crosses in figures 4.1 and 4.2 mark the “threshold point” for the VVP1 retrieval method. In figure 4.3 the applied standard deviation threshold is plotted as a function of the obtained number of available wind vectors for the VVP1 method. It is seen that a standard deviation threshold of 2.0 m/s should be applied to arrive at the threshold point.

The typical value for the rms vector differences between the Doppler radar and radiosonde wind vectors seems to lie between 2.0 and 3.0 m/s. According to the WMO guide on Meteorological Instruments and Methods of Observation the “rms vector differences between two error-free upper-wind observations at the same height (sampled at 300 m vertical resolution) will usually be less than 1.5 m/s if the measurements are simultaneous and are separated by less than about 5 km in the horizontal” (WMO, 1996). Given that the overlap in time and space between the Doppler radar and the radiosonde is far from perfect amongst others due to spatial averaging of the radar wind profile retrieval methods and to drifting of the radiosonde, the observed rms vector differences is satisfactory. Andersson (1998) has performed a verification of VAD wind profiles from C-band Ericsson Doppler radars against radiosonde profiles from a station at 10 km distance and he found rms vector differences between 3.5 and 4.0 m/s.

4.3 Doppler Wind Profiles against Hirlam

The weather radar wind profiles at De Bilt have also been verified against wind profiles from the nearest grid point of the Hirlam NWP model. Compared to the radiosonde profiles, the

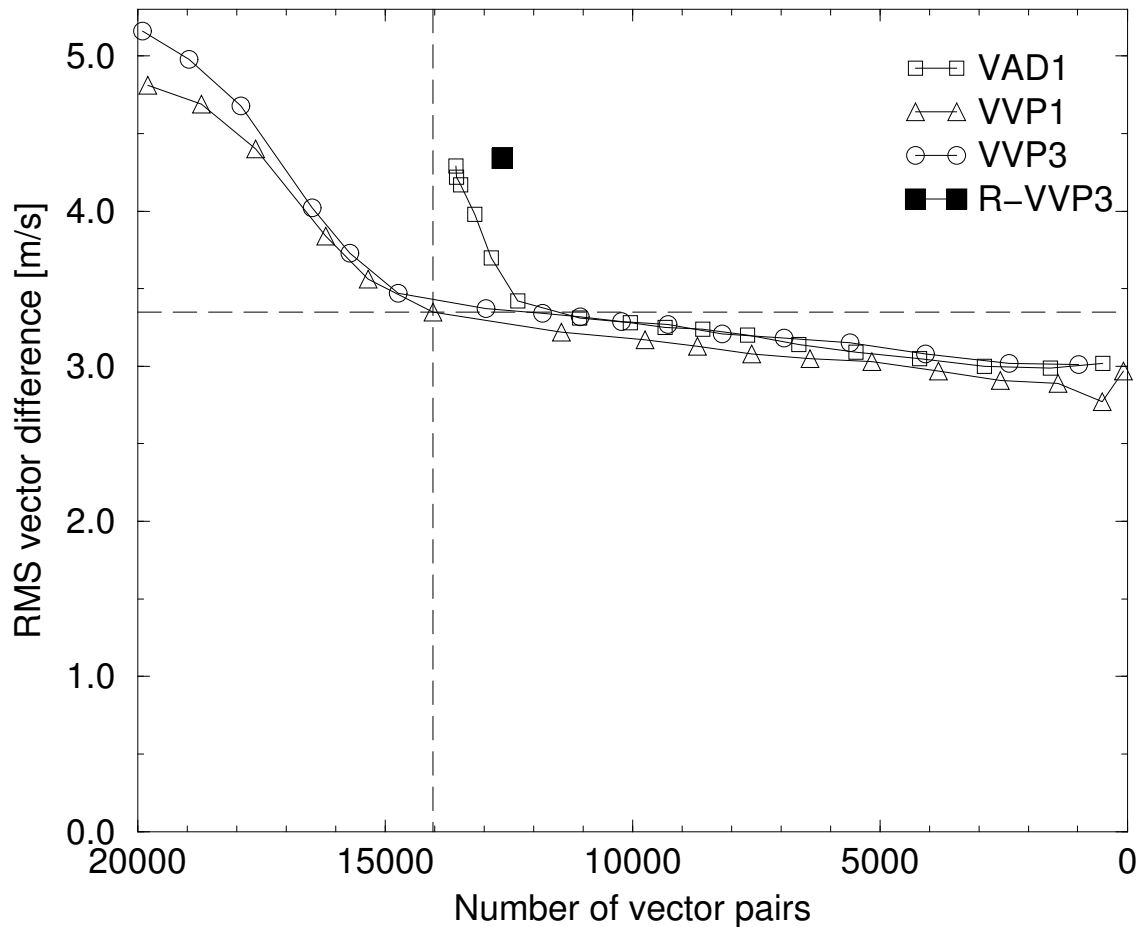


Figure 4.4: The rms vector differences between radar and Hirlam wind vectors as a function of the number of vector pairs. Curves for one Velocity Azimuth Display (VAD1) method, two Volume Velocity Processing (VVP1 and 3) methods, and the Rainbow VVP module (R-VVP3) are shown. The dashed cross marks the suggested threshold for the VVP1 wind vectors.

model profiles have the advantage that they represent roughly the same horizontal area as the radar wind profiles, that they are not influenced by individual clouds or storms, and that they are produced 8 times a day instead of 4 times (or currently only twice). In addition, the model profiles are available at all grid points and thus enable verification of radar profiles at sites where no radiosondes are launched. The vertical resolution of the Hirlam model is somewhat coarser than that of the radar wind profiles. Below 1 km altitude the Hirlam model has about 5 vertical levels, while between 1 and 6 km altitude the level spacing is roughly 500-600 m. Verification of weather radar wind profiles against model profiles can be considered a first step towards assimilation of the radar wind profiles in the Hirlam model.

Figure 4.4 shows the rms vector differences between the Doppler radar and Hirlam model wind vectors as a function of the number of vector pairs. Similarly to the plots of figures 4.1 and 4.2, the number of wind vector pairs has been varied by changing the threshold on the radial velocity standard deviation. The results are shown for a selection of the available wind profile retrieval methods: one velocity azimuth display method (VAD1), two volume velocity processing methods (VVP1 and VVP3), and the Rainbow VVP module. A comparison of figure 4.4 with the corresponding figures for the verification against radiosonde profiles reveals a striking resemblance. This is not that surprising because the radiosonde profiles are assimilated in the Hirlam model. The number of wind vector pairs is higher, because of the larger number of available Hirlam wind profiles. The typical value of the rms vector differences (2.5-3.5 m/s) is somewhat higher than that from the radiosonde verification. This may be due to the coarser vertical resolution of the Hirlam model profiles or to the negative wind speed bias of the Hirlam model at low altitudes due to the initialization scheme.

Despite the quantitative differences the verifications against the Hirlam profiles bring to mind the same conclusions as the radiosonde verifications. The VVP methods perform better than the VAD method, and the most simple volume velocity processing method (VVP1) performs best. The performance of the Rainbow VVP module is not as good as that of the VVP implementations. For further analysis of the wind profiles a suitable threshold on the radial velocity standard deviation has to be chosen. A standard deviation threshold of 2.0 m/s materialized from the analysis of the verification against radiosonde profiles. The dashed cross in figure 4.4 marks the point in the VVP1 verification curve where a standard deviation threshold of 2.0 m/s is applied. It appears that this threshold is also reasonably situated with respect to the bending point in the radar-Hirlam verification curves. In further analysis of the radar wind profiles, this 2.0 m/s threshold will be applied on the radial velocity standard deviation of the retrieved wind vectors.

4.4 Rejection of Radial Velocity Outliers

It has been mentioned in section 3.5 that the wind vector retrieval using singular value decomposition (SVD) is performed twice for every height layer. In between the SVD regressions

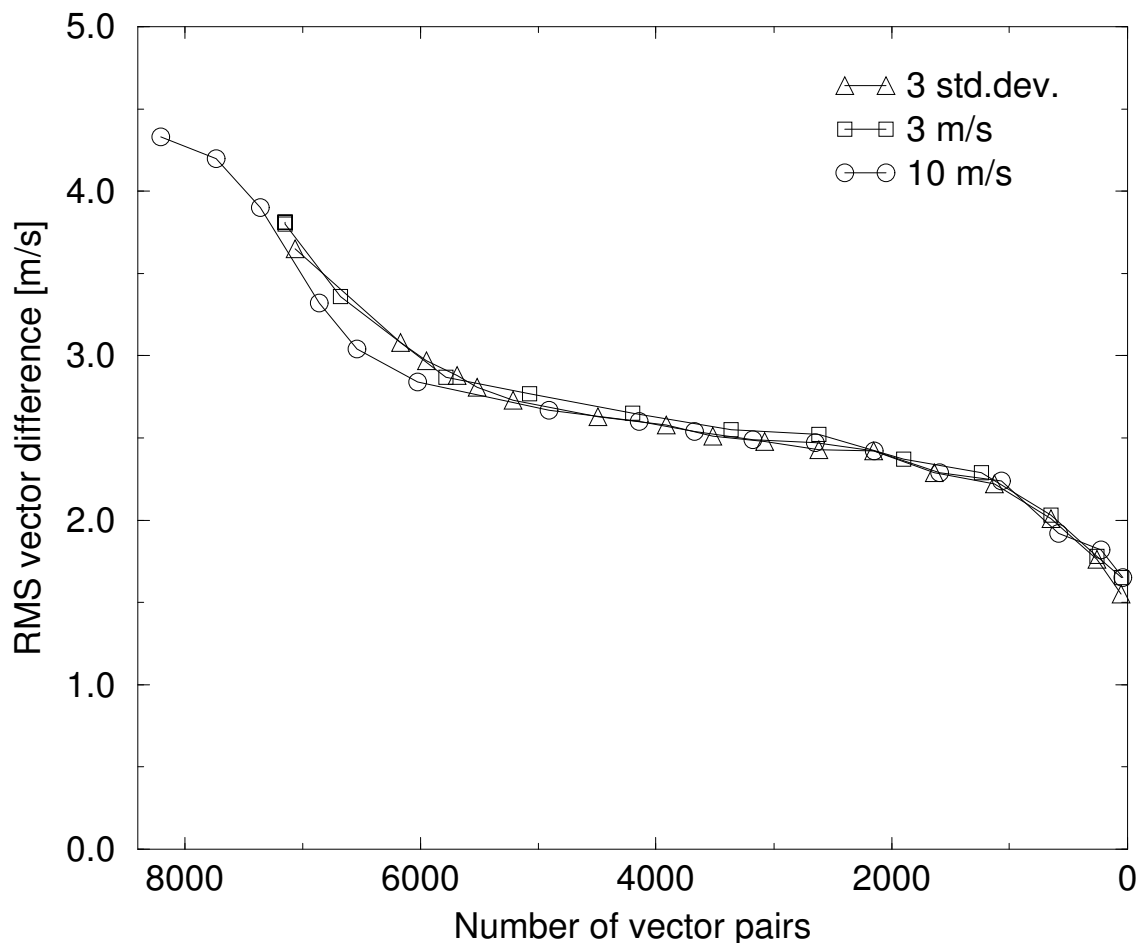


Figure 4.5: This figure shows the rms vector differences of the VVP1 and radiosonde wind vectors as a function of the number of available vector pairs. Different methods of velocity outlier detection have been applied during the wind vector retrievals (see text).

radial velocity outliers are removed from the volume scan data to improve the wind vector retrieval. The velocity outliers are detected by taking the difference of the radial velocity from the wind field model using the retrieved parameters and that from the volume scan data. The threshold value on this velocity difference can be set in different ways: using a fixed threshold or using a multiple of the retrieved standard deviation of the radial velocity as a threshold.

In figure 4.5 the rms vector differences of the VVP1 and radiosonde wind vectors is shown as a function of the number of available vector pairs. The threshold for removal of velocity outliers was determined in different ways: 3 times the standard deviation, a fixed value of 3 m/s, and one of 10 m/s. The verification results show that the method for setting the outlier threshold value is not very critical. The fixed threshold value of 10 m/s gives slightly better results than the 3 m/s threshold or the threshold value based on the standard deviation. This confirms the expected non-Gaussian distribution of the errors in the radial velocity data. The majority of the outliers will be due to isolated dealiasing errors which are characteristic for velocity data obtained using the dual-PRF technique (Holleman and Beekhuis, 2003). A fixed threshold value of 10 m/s for the removal of radial velocity outliers in between the two wind model fits will be applied.

Chapter 5

Performance of VVP Retrieval Technique

5.1 Availability of Wind Profiles

The combination of quality, availability, and error characteristics determines the impact of radar wind profiles for nowcasting or assimilation into NWP models. In the previous chapter a reasonable threshold for the radial velocity standard deviation has been selected. The impact of this choice on both the availability and the quality of the radar wind profiles will be investigated in this section and the next two sections, respectively. Using a standard deviation threshold of 2.0 m/s histograms of the wind speeds observed by Doppler radar using the VVP1 retrieval method have been constructed for three different height ranges. The constructed histograms for the 0-2 km, 2-4 km, and 4-6 km height ranges are shown in figure 5.1. The vertical axis represents the wind vector count per 1 m/s-wide bin using all available radar wind profiles between 1 October 2001 and 30 June 2002. The vertical bars represent the mean radiosonde wind speeds over the same period. Comparing the histograms for the three height ranges, it is evident that the total number of available wind vectors and the mean wind speed are decreasing and increasing, respectively, with increasing height. The vertical dashed line marks the maximum unambiguous velocity of the Doppler scans using the dual-PRF technique (see section 2.6). It is remarkable that for the upper height range a significant number of wind vectors with speeds above the unambiguous velocity are observed. For these high wind speeds the observed VAD curves (see figure 3.1) will be distorted: radial velocities larger than the unambiguous velocity will be aliased and shifted by 80 m/s. Apparently the wind profile retrieval method is capable of dealing with these velocity outliers.

In table 5.1 the quantitative results of the histogram analysis have been collected. The table lists for 1 km height ranges the fraction of the number of available wind vectors to the maximum number of vectors. This “availability fraction” decreases from 0.39 in the lowest height range to 0.16 in the highest height range. In the boundary layer the radar radiation is scattered by precipitation, refractive-index gradients, insects and birds (Wilson et al., 1994), and above the boundary layer the radiation will be scattered by precipitation only. During

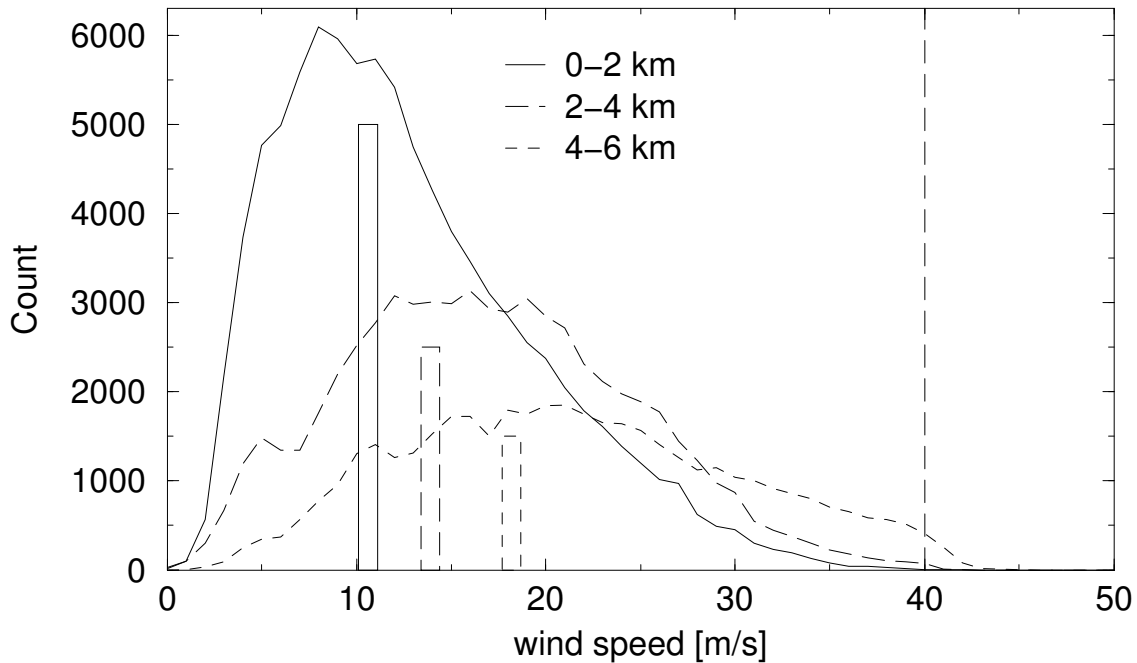


Figure 5.1: This figure shows histograms of the observed wind speeds for three different height layers and using wind speed bins of 1 m/s. The wind speeds are obtained from the radar using the VVP1 retrieval method and a standard deviation threshold of 2.0 m/s. The vertical bars represent the mean wind speeds as obtained from the radiosonde observations over the same period.

Table 5.1: This table contains the quantitative results of the histogram analysis for 1 km height ranges. For each height range, the total number of available wind vectors (Count), and the fraction number of available vectors to the maximum number (Availability) are listed. The maximum number of wind vectors is the product of the number of profiles (22610) and the number of layers per height range (5).

Height	Count	Availability
0-1 km	44392	0.393
1-2 km	46184	0.409
2-3 km	34308	0.303
3-4 km	28072	0.248
4-5 km	24049	0.213
5-6 km	18310	0.162

the verification period, the synoptical station at De Bilt has reported precipitation in 925 out of 6552 possible cases, i.e., a precipitation occurrence fraction of 0.141. It is evident from table 5.1 that the wind vector availability fraction converges to this fraction with increasing height. The observed availability at low altitudes (0-2 km) is considerably lower than the 0.83 and 0.64 at 925 and 850 hPa, respectively, as reported by Andersson (1998). His rms vector differences are also considerably higher than the values in figure 4.1, indicating that a different balance between availability and quality was chosen.

5.2 Quality as a function of Wind Speed

A reasonable threshold for the radial velocity standard deviation has been selected previously. Using this standard deviation threshold the performance of the wind profile retrieval methods has been investigated using several quality measures. In this section the performance of the VVP1 retrieval method as a function of the wind speed will be analyzed. For this, the collected pairs of wind vectors from the VVP1 retrieval and radiosonde with matching time and height coordinates have been grouped according to the radiosonde wind speed. As stated previously, radiosondes are typically launched 30 minutes too early and therefore radiosonde profiles of e.g. 12 UTC are compared with Doppler wind profiles from 11:30 UTC. Quality parameters, like the root-mean square (rms) vector differences, the bias and standard deviation of wind speed and direction, have been calculated for all wind speed groups.

The results of the quality analysis as a function of wind speed (group) are presented in figure 5.2. The upper part of the figure shows the rms vector differences between the VVP1 and the radiosonde wind vectors as a function of the radiosonde wind speed. Note that these rms vector differences differ from those in figures 4.1 and 4.2, because the standard deviation threshold has now been applied to quality control the retrieved wind vectors. When the selected wind speed is increased from the lowest to the highest group, the rms vector differences is slowly increasing from 2 to 3 m/s. This increase of the rms vector differences is attributed to the increasing horizontal separation between the radiosonde and radar observations with increasing wind speed.

The middle part of figure 5.2 displays the bias and standard deviation of the wind speeds from the VVP1 retrieval with respect to the radiosonde wind speeds. It is evident that the wind speed bias is generally smaller than 0.5 m/s and positive, i.e., the radar wind speeds are slightly higher than those of the radiosonde. The wind speed bias is much smaller than the corresponding standard deviation, and it is therefore considered to be within acceptable limits. The relatively large positive bias for the lowest wind speed group is most likely due to the rejection of radial velocities below 2 m/s (see section 3.5). For the highest wind speed group, the bias is -1 m/s which is probably caused by the limited unambiguous radial velocity (40 m/s) of the radar. The required accuracy (standard deviation) of upper air wind speed measurements is 1 m/s according to the WMO guide on Meteorological Instruments and Methods of Obser-

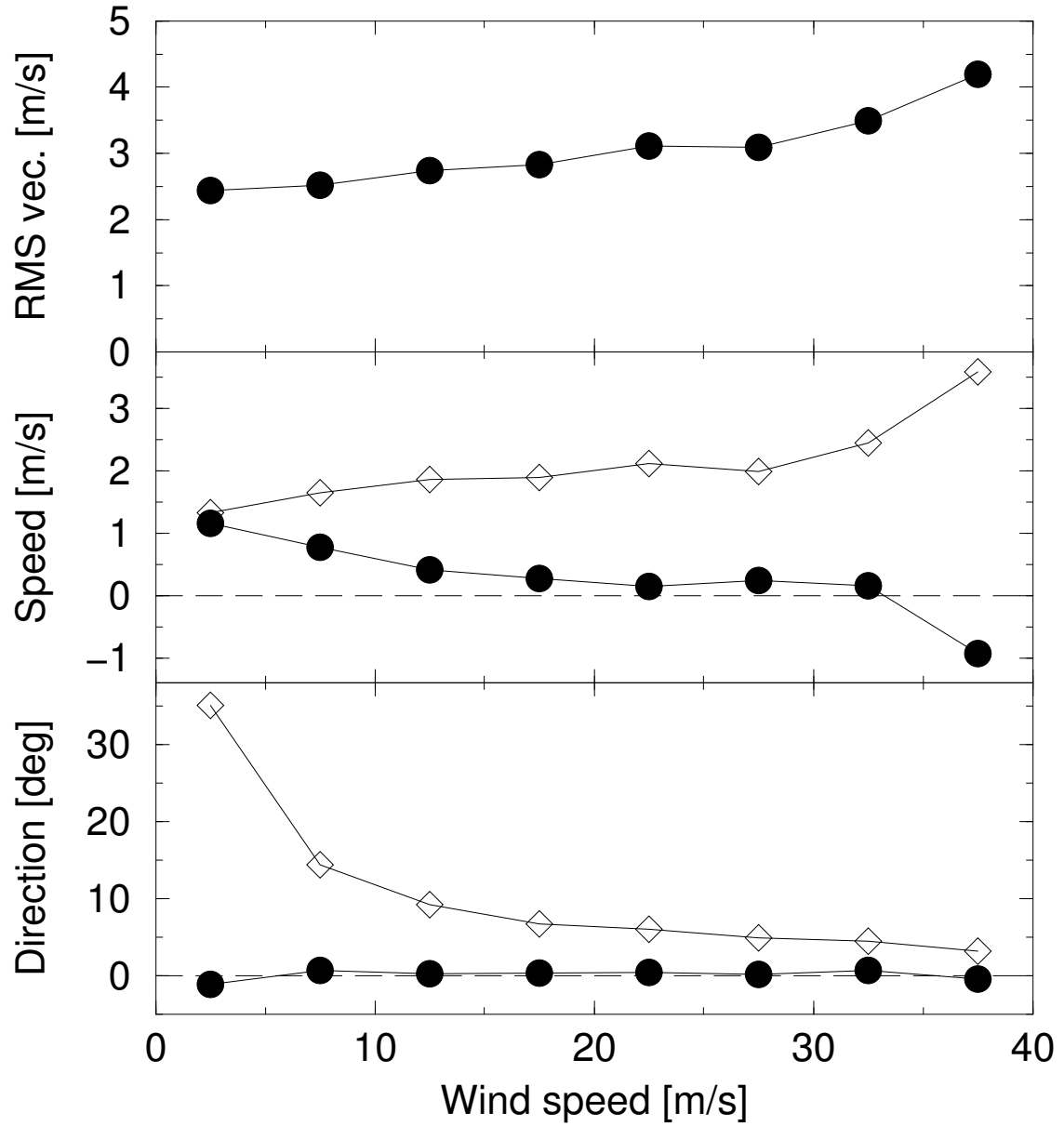


Figure 5.2: This figure shows the rms vector differences in the upper frame, the bias (\bullet) and standard deviation (\diamond) of the wind speed (middle frame), and the bias (\bullet) and standard deviation (\diamond) of the wind direction (lower frame) as a function of wind speed. These quality parameters have been obtained from the verification of VVP1 wind vectors against those from the radiosonde.

vation (WMO, 1996). This confirms that the observed wind speed bias is within acceptable limits, and suggests that the observed standard deviation, which is deduced from a comparison between two measurements, just satisfies the accuracy requirements.

The bias and standard deviation of the wind direction from the VVP1 retrieval with respect to that of the radiosonde are shown in the lower part of figure 5.2. The bias of the wind direction is usually less than 1 degree and thus is negligible. For the standard deviation of the wind direction a strong dependence on the wind speed is observed. This standard deviation drops from a rather high value of about 35 degrees at low wind speeds to a low value of only 3 degrees at high wind speeds. The observed dependence of the standard deviation on the wind speed suggests that the errors in the Cartesian wind field components, the originally retrieved parameters, are (approximately) constant. The wind direction is determined from the ratio of the horizontal wind field components and this ratio has a larger error for lower wind speeds. The required accuracy (standard deviation) of upper-air wind direction measurements is 5 and 2.5 degrees for wind speeds below and above 15 m/s, respectively (WMO, 1996). The bias of the observed wind direction is within acceptable limits. The observed standard deviation is caused by errors in radar and radiosonde measurements, and by sampling differences. It appears that for wind speeds above 10 m/s the Doppler radar is capable of providing wind profiles which satisfy the stringent accuracy requirements by WMO.

5.3 Quality as a function of Height

Another and maybe more intuitive way of grouping the wind profile verification data is according to the height of the retrieved wind vectors. In this section the performance of the VVP1 retrieval method and the Rainbow VVP module will be analyzed by verification against radiosonde and the Hirlam model. The collected pairs of wind vectors matching in time and height have been grouped into 1 km thick height layers and several quality measures have been calculated. The results are presented as profiles in figures 5.3 to 5.7.

Figure 5.3 shows profiles of the bias and standard deviation of the wind speed and direction for the VVP1 retrieval method. These quality measures have been obtained from verification against radiosonde wind profiles. Because the mean wind speed increases with height (see figure 5.1), the verification results presented in this figure are strongly correlated to those in figure 5.2 and similar features can indeed be seen. The wind speed bias is slightly positive at all heights and less than 0.5 m/s. The standard deviation of the wind speed is slowly increasing from 1.5 m/s at low altitude to about 2.0 m/s at the highest altitude. The same tendencies but more pronounced are evident from the middle part of figure 5.2. The wind direction bias shows a remarkable sign change between 3 and 4 km altitude. This sign change is not observed in the wind direction bias as a function of wind speed (see lower part of figure 5.2), and it therefore must originate from a true (unexplained) height effect. The decrease of the standard deviation of the wind direction with increasing height is similar to that with increasing wind speed, but

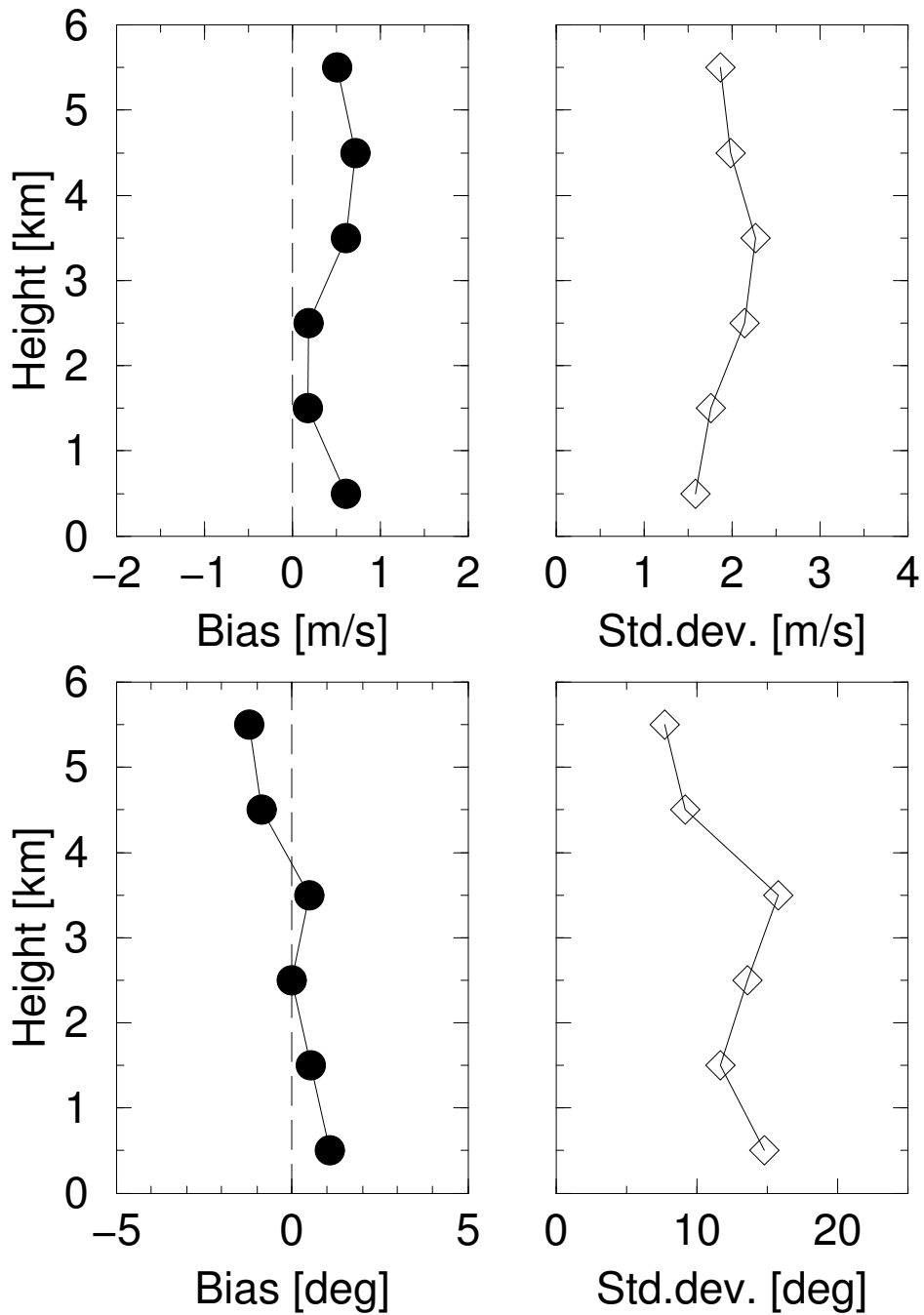


Figure 5.3: This figure shows profiles of the bias and standard deviation of the wind speed and direction as obtained from verification of VVP1 against radiosonde.

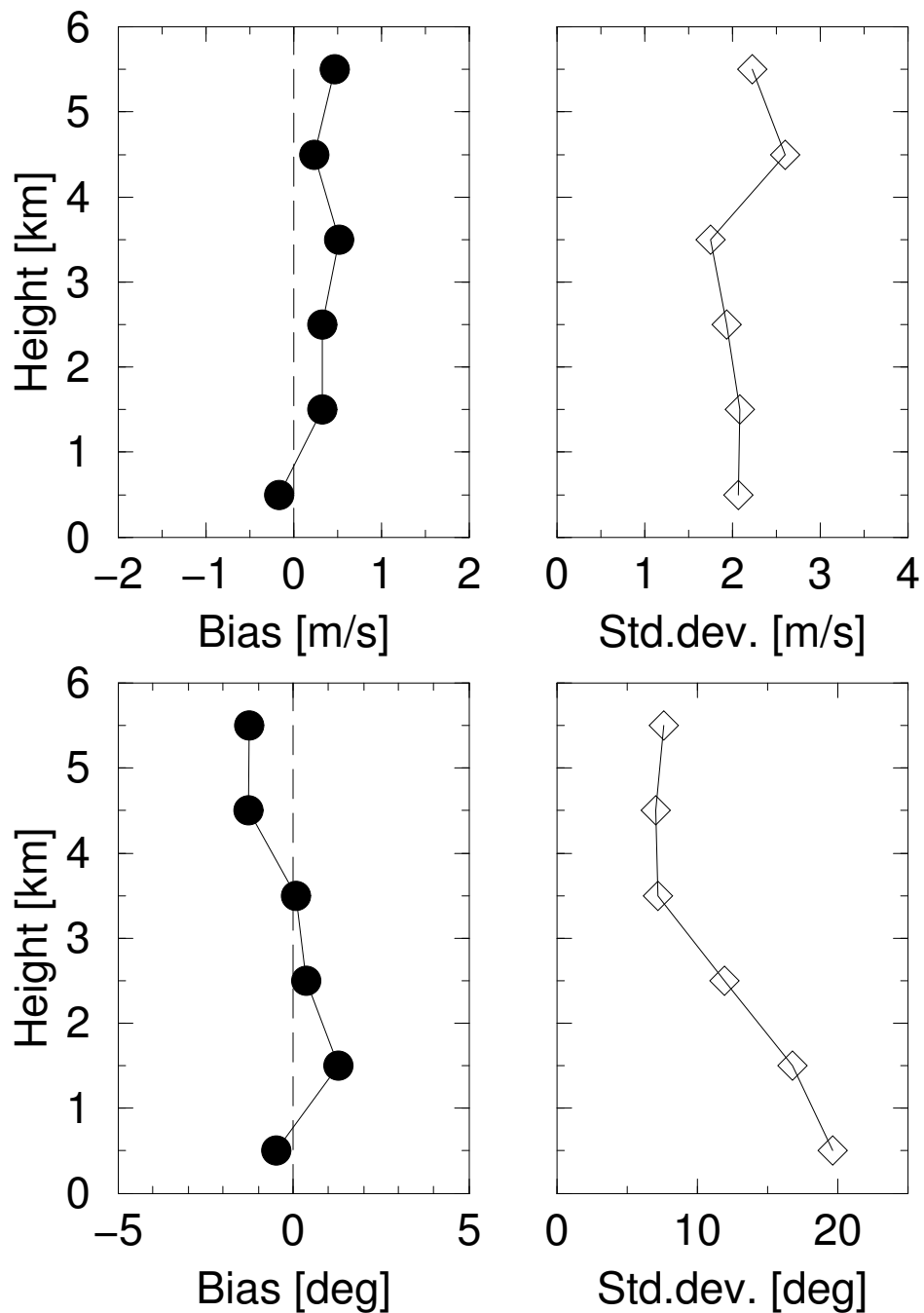


Figure 5.4: This figure shows profiles of the bias and standard deviation of the wind speed and direction as obtained from verification of Rainbow VVP module (R-VVP3) against radiosonde.

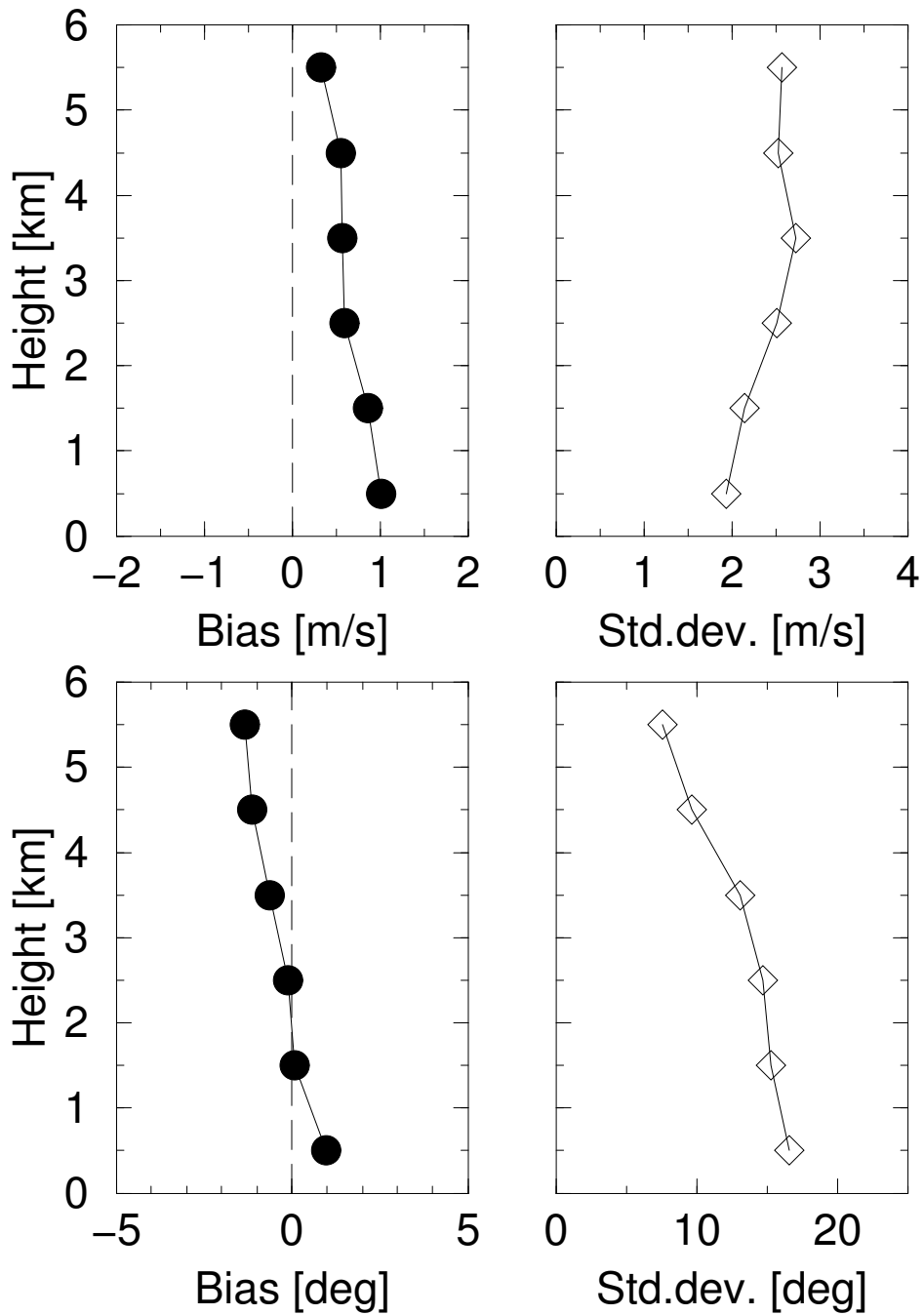


Figure 5.5: This figure shows profiles of the bias and standard deviation of the wind speed and direction as obtained from verification of VVP1 against Hirlam.

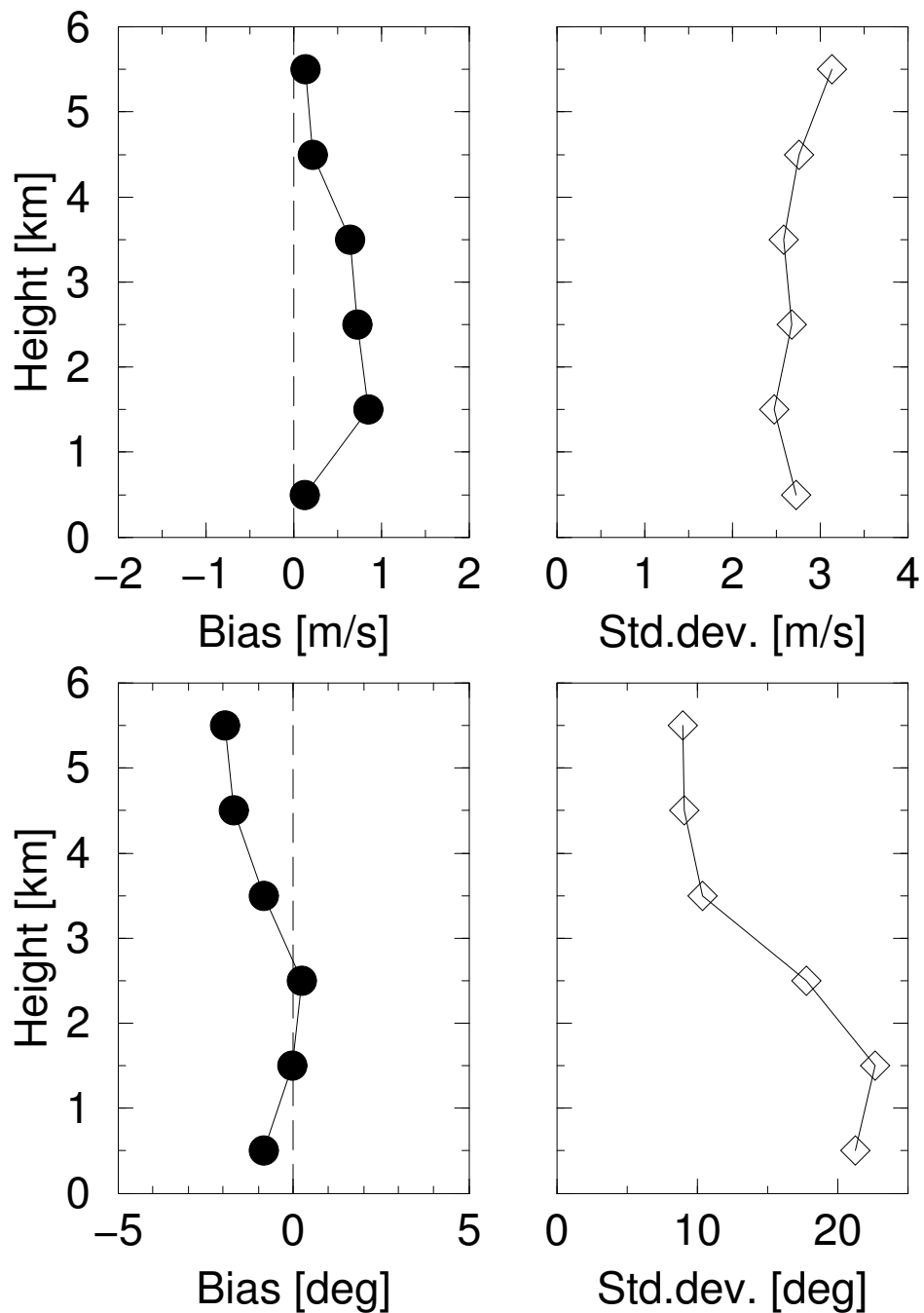


Figure 5.6: This figure shows profiles of the bias and standard deviation of the wind speed and direction as obtained from verification of Rainbow VVP module against Hirlam.

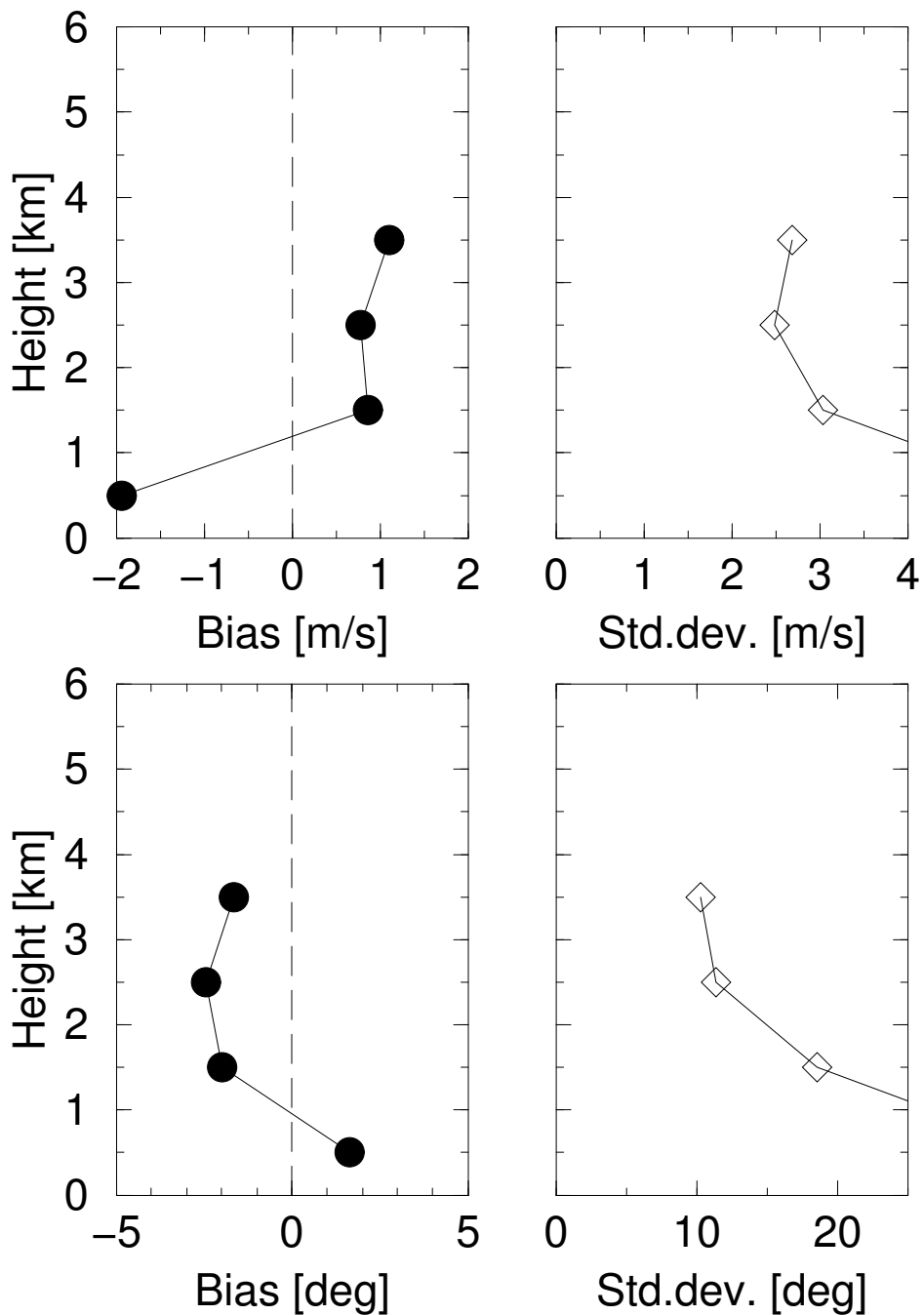


Figure 5.7: This figure shows profiles of the bias and standard deviation of the wind speed and direction as obtained from verification of Rainbow VVP module **at Den Helder** against Hirlam.

it has a smaller amplitude.

The bias and standard deviation profiles obtained from the verification of the Rainbow VVP module against the radiosonde observations are shown in figure 5.4. Comparing the profiles in this figure with those in the previous figure, the bias profiles of both wind speed and direction match very well and the standard deviation profiles are shifted to higher values. In addition, the speed and directional bias of the R-VVP3 wind vectors are negative below 1 km altitude. The higher standard deviations and the remarkable discrepancy between the biases of the VVP1 and R-VVP3 wind vectors below 1 km are probably due to the absence of standard deviation thresholding after the final fit and the less stable regression algorithm in the Rainbow VVP module.

The retrieved wind profiles have also been verified against profiles from the Hirlam model. Figures 5.5 and 5.6 show the bias and standard deviation profiles from the verification of the VVP1 retrieval method and the Rainbow VVP module, respectively, against the Hirlam model. Comparing these two figures with the corresponding figures from the verification against radiosonde, reveals a good qualitative and a fair quantitative match of the bias and standard deviation profiles obtained with the different verification data. All obvious features of the bias profiles, like the positive speed bias and the sign change of the directional bias, are reproduced using the Hirlam data for verification. At low altitudes, the observed speed bias is larger than for the verification against radiosonde which is probably due to a negative speed bias in the initialized analyzes of Hirlam. In addition the standard deviation profiles of wind direction match quantitatively, but those of wind speed are shifted to somewhat higher values. This quantitative difference is in correspondence with the larger rms vector differences for verification against the Hirlam model as presented in section 4.3. Thus for De Bilt, verification of wind profiles against the Hirlam model provides the same qualitative insights and almost the same quantitative results as verification against radiosonde.

For the radar in Den Helder, Rainbow VVP wind profiles and corresponding Hirlam profiles are available. Figure 5.7 shows the profiles of bias and standard deviation from the verification of the R-VVP3 module against Hirlam for the Den Helder radar. At first glance it is striking that the profiles only go up to 4 km altitude which is due to the limitation of the scan strategy of the radar in Den Helder (see section 2.6). In the next section the quantitative impact of this limitation will be investigated further. Other striking features are the large wind speed bias, and very large standard deviations below 1 km altitude. This is probably due to the inhomogeneous environment, the radar is located on land but large water surfaces are nearby in many directions (< 5 km). These land-sea transitions are not fully represented in the Hirlam model due to the larger grid spacing. In addition these large standard deviations may be caused by interference from sea clutter in the lowest elevation beams.

5.4 Removal of Elevations

Up to now velocity scan data from 10 elevations have been used to retrieve the radar wind profiles. The elevations are listed in table 2.1. For development of operational scanning strategies it is important to know whether data from all 10 elevations are really needed to obtain wind profiles of sufficient quality. In addition the radar in Den Helder is currently not allowed to use elevations above 12 degrees. A demonstration of the impact of this limitation on the quality and availability of the radar wind profiles may provide an impulse to re-open the negotiations with the naval air base in Den Helder.

The radar wind profiles at De Bilt have been re-calculated from volume scan data using the VVP1 retrieval method and removing data from selected elevations. When the elevations in the volume scans as listed in table 2.1 are numbered from 0 to 9, the wind profiles have been re-calculated for the following six scenarios:

Null: Velocity scan data from all elevations are used. This scenario is included for reference purposes.

Zero: Scan data from elevation “zero” (0.5 degrees) are excluded from the wind profile retrieval. It is expected that velocity data from this low elevation are contaminated by (sidelobe) clutter and that wind profile retrieval may benefit from this exclusion.

Nine: Scan data from elevation “nine” (25 degrees) are excluded from the wind profile retrieval. Data from this high elevation may be contaminated by the inhomogeneity of the terminal velocity of the hydrometeors and of (strong) updrafts (see section 3.1).

Even: Velocity scan data from the five even numbered elevations have been excluded from the wind profile retrieval. The impact of the removal of 50% of the scan data on the quality and availability of the wind profiles can be investigated using this scenario.

Odd: Velocity scan data from the five odd numbered elevations have not been used for the wind profile retrieval. Use is the same to that of the previous scenario.

DenHelder: Scan data from the 3 highest elevations (>12 degrees) have not been used. In this scenario the “Den Helder limitation” is also applied to De Bilt radar, and the impact of this limitation can be investigated.

The availability fractions and rms vector differences with respect to radiosonde wind data as a function of height are listed in tables 5.2 and 5.3, respectively, for the six scenarios. The removal of the lowest elevation from the scan data (scenario **zero**) improves the quality, i.e., reduces the rms vector differences, of the retrieved wind vectors below 4 km altitude, but it slightly reduces the availability. This finding supports the idea that the quality of radial velocity data from the lowest elevation is of poor quality at short ranges due to sidelobe clutter. The removal of the highest elevation (scenario **nine**) has a small effect on the availability, but it

Table 5.2: In this table the wind vector availability fractions are listed as a function of height for the six scenarios (see text). A standard deviation threshold of 2.0 m/s has been used to quality control the retrieved wind vectors. The number of wind vectors corresponding to an availability fraction of 1 is the product of the number of profiles (22610) and the number of layers per height range (5).

Height	Null	Zero	Nine	Even	Odd	DenHelder
0-1 km	0.39	0.36	0.39	0.34	0.37	0.39
1-2 km	0.41	0.40	0.40	0.38	0.37	0.38
2-3 km	0.30	0.30	0.29	0.29	0.29	0.24
3-4 km	0.25	0.24	0.23	0.23	0.24	0.19
4-5 km	0.21	0.21	0.20	0.20	0.21	0.14
5-6 km	0.16	0.16	0.15	0.16	0.16	0.04

Table 5.3: In this table the rms vector differences between the VVP1 wind vectors and those of the radiosonde are listed as a function of height for the six scenarios (see text). A standard deviation threshold of 2.0 m/s has been used to quality control the retrieved wind vectors.

Height	Null	Zero	Nine	Even	Odd	DenHelder
0-1 km	2.37	2.23	2.37	2.27	2.44	2.37
1-2 km	2.47	2.40	2.47	2.48	2.61	2.46
2-3 km	3.02	2.94	2.88	3.02	3.04	2.87
3-4 km	3.37	3.32	3.23	3.30	3.36	3.24
4-5 km	3.15	3.16	3.13	3.20	3.12	3.14
5-6 km	3.10	3.11	3.05	3.13	3.19	3.12

gives a clear improvement of the quality of the retrieved wind vectors above 2 km altitude. Data from the highest elevation (25 degrees) is contaminated by a larger inference from the inhomogeneity of the vertical velocity.

For the **even** and **odd** scenarios the number of available elevations and thus the scanning time has been reduced by a factor of two. This drastic reduction of the scanning time has only a minor (negative) impact on the availability and rms vector differences of the retrieved wind vectors. The VVP1 retrieval method performs equally well for the two reduction scenarios, but it appears that the rms vector differences are somewhat better for the **even** scenario and that the availability is slightly better for the **odd** scenario.

Application of the **DenHelder** scenario removes the elevations above 12 degrees and thus simulates the “Den Helder limitation” for radar in De Bilt. It is evident from table 5.2 that this limitation has a major impact on the availability of wind vectors above 3 km altitude. The availability fraction between 5 and 6 km altitude, for instance, drops from 0.16 to 0.04 which is about 75%. The impact on the quality, i.e., on the rms vector differences, of the retrieved wind vectors is small (see table 5.3). This is in accordance with the outcome for the **even** and **odd** scenarios that the quality of the retrieved wind vectors is not very sensitive to the number of elevations. Between 2 and 5 km altitude the rms vector differences for the **DenHelder** scenario are smaller than the values for the **null** scenario. This may be due to an increasing interference from the inhomogeneity of the vertical velocity at higher elevations.

5.5 Outliers: Bird Migration?

When comparing Doppler radar wind profiles to radiosonde or Hirlam model profiles, groups of clearly outlying wind vectors are observed occasionally. In figure 5.8 a time series of VVP1 and Hirlam wind profiles for 28 October 2001 are shown in black and blue, respectively. The VVP1 wind vectors in the upper time-height plot are obtained using the default standard deviation threshold of 2.0 m/s. It is evident that the majority of the VVP1 wind vectors matches the Hirlam reference wind vectors almost perfectly and that a group of VVP1 wind vectors is clearly deviating from the reference vectors between 19 and 21 UTC. Given that the outlying vectors point towards south and that the wind profiles are recorded in autumn, these outlying “wind” vectors are attributed to interference due to bird migration.

It is well-known that non-hydrometeor targets such as insects and birds are also detected by Doppler radar. While some insects can provide a help in defining the boundary layer wind, birds and actively flying insects, like moths or grasshoppers, can be a major problem for wind retrieval algorithms (Riley, 1999; Koistinen, 2000; Collins, 2001). Alternatively, (weather) radar can be employed to study bird movements and flight behavior of insects in the atmosphere. Eastwood (1967) pioneered in the field of radar ornithology in the late sixties and showed that radar can be used to detect, monitor, and quantify bird movements. During the same period, Schaefer (1969) for the first time used a radar to study the migration of insects

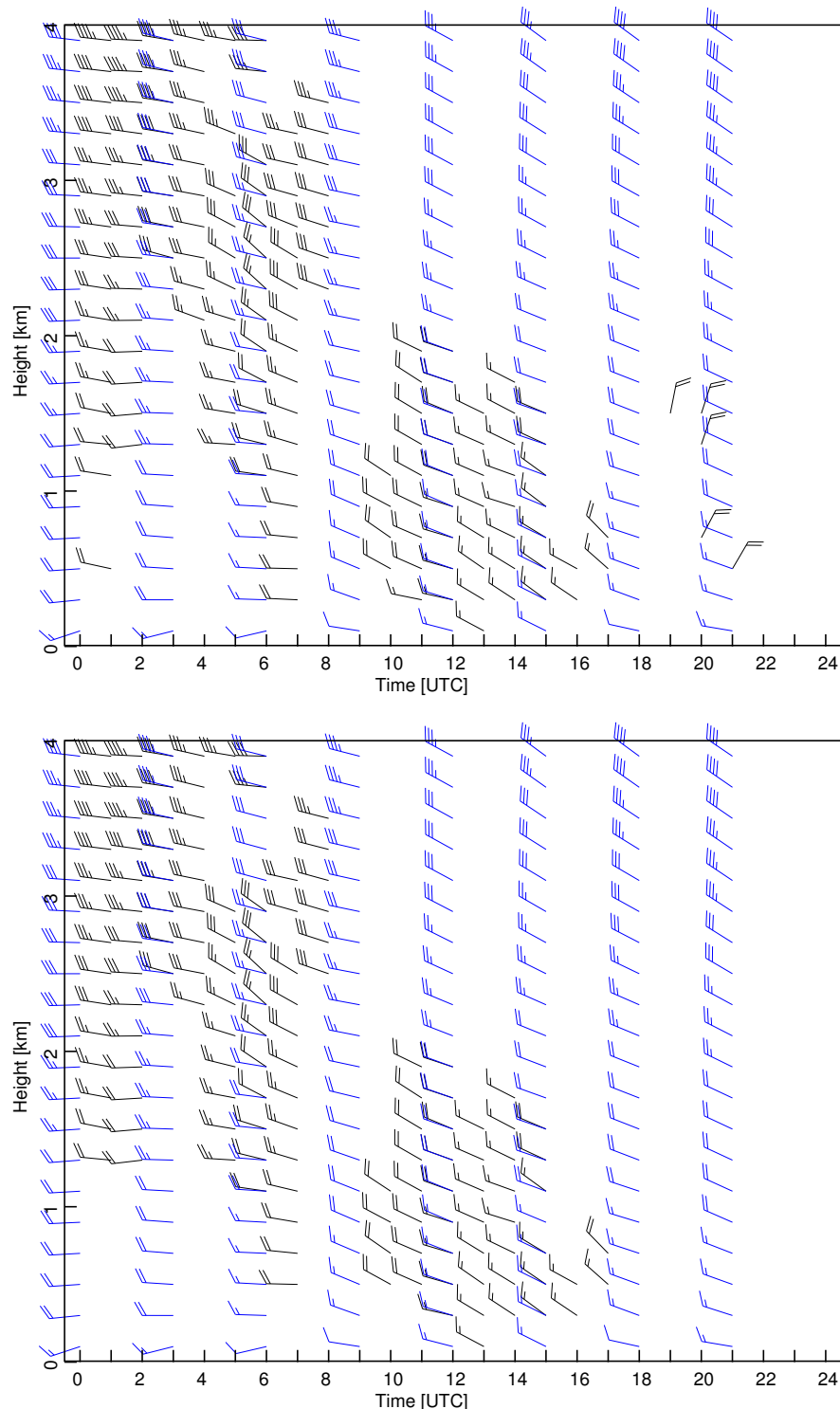


Figure 5.8: Two time-height plots with the hourly retrieved wind vectors using the VVP1 technique for 28 October 2001. The upper time-height plot is obtained using the default standard deviation threshold of 2.0 m/s and the lower plot using a threshold of 1.8 m/s. The wind profiles from the Hirlam model are overlaid in blue. Wind speed and direction are indicated by wind vanes. Each full barb represents a wind speed of 5 m/s and each triangle a wind speed of 25 m/s.

in the Sahara. A detailed overview of the relevant properties of bird migration for radar meteorology is presented by Koistinen (2000). Depending on the species, migrating birds have an air speed between 7 and 20 m/s. The track vector of a migrating bird, which is equal to the outlying “wind” vector, is the sum of the environmental wind vector (tail wind) and the heading vector of the bird. The heading is usually such that it (partly) compensates the wind drift from the final goal. The tail wind plays a crucial role in bird migration, because it determines the intensity of the migration and the distribution of the cruising heights. In Northern Europe typical cruising heights are between 0.5 and 2 km and in the Mediterranean region flight heights up to 4 km can be found. Heavy bird migration occurs when the 10 m wind speed is below 8 m/s and the wind direction is favorable. When the 10 m wind speed is above 11 m/s, the bird is unable to compensate the wind drift and the risk of dangerous wind gusts near the ground increases rapidly. The other important meteorological factor influencing the intensity of the migration is precipitation. Heavy precipitation may directly influence the flying capability of a bird, and in addition it hampers the available navigation senses (Koistinen, 2000).

Using the afore mentioned properties and wind profiles from other sources, a manual diagnosis of birds migration and/or outlying “wind” vectors is not very difficult. An automatic detection of bird migration based on radar data only is not straightforward. In the lower frame of figure 5.8 a time-height plot of VVP1 retrieved wind profiles for the same day as the upper frame but with a non-default standard deviation threshold of 1.8 m/s is shown. It is evident that application of this slightly more stringent threshold eliminates the outlying “wind” vectors from the profiles in this case. This is in agreement with the observation of Koistinen (2000) that the standard deviation of the radial velocity determined from the wind profile retrieval is larger in bird migration than in rain. The application of a more stringent threshold on the standard deviation is not without a cost. From figure 4.3 it can be deduced that the 10% lower threshold leads to a 6% reduction of the number of available VVP1 wind vectors. Wind vectors from clear-air return also have a relatively large standard deviation and these wind vectors will thus be removed primarily. As detailed before the quality and availability of wind profiles are coupled, and the optimum setting of standard deviation threshold will, therefore, depend on the application of the profiles. For nowcasting purposes a high availability of the wind profiles is most important, while for assimilation in NWP models the quality of the profiles is the main issue.

An attempt has been made to find a method to eliminate outlying “wind” vectors due to bird migration without reducing the availability of the wind vectors significantly. The proposed method is based on the assumed difference in the spatial structure of the radial velocity scan data for precipitation and migrating birds. During precipitation large continuous areas with valid radial velocity data are usually present in volume scan data, and in contrast migrating birds give rise to scattered groups of range bins with valid data. As part of the correction algorithm for dual-PRF velocity data a group-size filter has been developed which removes groups with valid data consisting of less than a minimum number of range bins from the scan data (Holleman and Beekhuis, 2003). This group-size filter has been applied to remove the

Table 5.4: Elimination of outlying “wind” vectors due to bird migration using group-size filtering and reduction of standard deviation threshold. To favor the bird migration “wind” vectors, only vectors between 1 and 4 km altitude have been considered. The table lists the applied standard deviation threshold (std.dev.), the minimum group-size after filtering (size), the rms vector differences against Hirlam wind profiles matching within 1.5 hour (rms), the total number of retrieved wind vectors (total), and the number of outlying wind vectors, i.e., vectors with at least 8 m/s offset in the north-south direction with respect to Hirlam (outliers).

Std.dev.	Size	rms	Total	Outliers
2.0	0	3.6	100456	541
2.0	5	3.6	91355	570
2.0	10	3.6	87461	572
2.0	15	3.6	85407	569
2.0	20	3.6	83658	535
2.0	25	3.6	82542	525
1.8	0	3.5	95632	418
1.5	0	3.4	83927	280
1.0	0	3.1	47289	87

scattered groups of range bins, assumed to be due to migrating birds, from the volume scan before retrieval of the wind profile using the VVP1 technique. Minimum group sizes between 5 and 25 range bins have been applied in different runs. It is found that application of the group-size filter has a negligible impact on the average quality and availability of the VVP1 wind vectors (see table 5.4). The outlying “wind” vectors due to bird migration are recognized by a large offset of the north-south wind component (8 m/s) with respect to Hirlam profiles (Collins, 2001) and a height between 1 and 4 km. The results of this experiment are listed in table 5.4. Unfortunately, it is evident from the table that application of the group-size filter does not reduce the number of outlying vectors. In contrast, the standard deviation threshold provides an adequate means to control the number of outlying wind vectors.

Chapter 6

Conclusions and Recommendations

In this scientific report an introduction to Doppler velocity observations and the optimized settings of the Doppler radar are presented. In addition, the principles of wind profile retrieval methods are introduced and different versions of the VAD and VVP wind profile retrieval techniques have been described. Finally, an intercomparison of the different implementations of the VAD and VVP retrieval techniques and an extensive verification of VVP wind profiles using radiosonde and Hirlam profiles have been performed. It is concluded that Doppler radars can provide good quality wind profiles with a reasonable availability, and operational application of the Doppler radar wind profiles is recommended.

The settings of the Doppler radar have been optimized by adjusting the scanning strategy and the parameters of the radar signal processor. The choice for the applied Doppler clutter filter and the values of threshold qualifiers on the signal processor are based on the outcome of dedicated experiments. Going through the equations for the wind profile retrieval techniques, it is obvious that several stages of simplification can be applied to the VAD and VVP methods. The intercomparison of these different implementations of the retrieval methods and the Rainbow VVP module using radiosonde and Hirlam reference profiles revealed that the VVP methods perform better than the VAD methods. In contrast to a VVP retrieval, where all available scan data within range is quality controlled at once, all velocity-azimuth circles are quality controlled individually during a VAD retrieval, and this results in a higher rejection rate. Furthermore, it was found that the most simple implementation of the VVP retrieval method, i.e., using only 3 wind field parameters, provides the best horizontal wind data. Due to the non-orthogonality of the basis functions, addition of higher-order functions with (small) linear dependencies may cause fluctuations of the retrieved parameters. The performance of the Rainbow VVP module is comparable with the developed VVP implementations. The availability and the quality of the wind profiles are coupled as expected, and a threshold on the standard deviation of the radial velocity as determined by the retrieval method can be applied to shift between high availability and high quality. A standard deviation threshold of 2.0 m/s seems a reasonable compromise and has been applied throughout this report.

An availability fraction of VVP1 wind vectors of about 0.39 is found in the lowest 1 km of the troposphere, and at 5-6 km altitude the availability has dropped below 0.16 which is approaching the fraction of observed precipitation in De Bilt during the verification period (0.14). In the boundary layer the radar radiation is scattered by precipitation, refractive-index gradients, insects and birds, while above this layer the radiation is scattered by precipitation only. Verification as a function of wind speed of the VVP1 wind vectors against radiosonde data revealed that the accuracy of the retrieved wind speeds satisfies the WMO requirements for upper-air wind measurements and that the accuracy of the retrieved wind directions meets the requirements only above wind speeds of 10 m/s. At the cost of availability, application of a more stringent standard deviation threshold can further improve the accuracy of the retrieved wind vectors. Verification of the VVP1 and Rainbow VVP wind profiles as a function of height using radiosonde and Hirlam reference profiles showed that use of Hirlam leads to same qualitative results and slightly different values for bias and standard deviation. The experiments with selective removal of elevations from volume scan data revealed that the VVP1 retrieval method is generally not very sensitive to the loss of elevations, but that the elevation limitation for the Den Helder radar has a large impact on the availability fraction above 3 km altitude. Bird migration is a potential problem for Doppler radar wind profiles. A method for removal of outlying wind vectors due to bird migration based on the assumed spatial structure of the radial velocity scan data for precipitation and migrating birds has been tested without success, but a lowering of the standard deviation threshold may offer a way out for some applications.

Based on the findings presented in this report, operational application of the Doppler radar wind profiles is highly recommended. Before operational application of the Rainbow VVP module for retrieval of wind profiles, a few improvements and extensions should be considered:

1. Implementation of an option to change the number of wind field parameters used by the Rainbow VVP module from 3, 6, to 9 parameters and thus increase the complexity of the VVP retrieval.
2. Extension of the retrieval output of the Rainbow VVP module from wind speed and direction to include the vertical velocity, the number of fitted data points, and the radial velocity standard deviation. Especially the standard deviation can be employed to (further) quality control the retrieved wind vectors (depending on the application, e.g., assimilation in NWP).
3. Apply of the standard deviation threshold after the second wind model fit instead of after the first fit.
4. Change the regression algorithm from the solution using standard normal mode analysis to the more accurate solution by Singular Value Decomposition (SVD). SVD is the cure for round-off errors and for almost singular sets of equations.

5. Re-open the negotiations with naval air base in Den Helder on the 12 degree elevation limitation for the Den Helder radar.
6. Implement a conversion of the wind profiles to BUFR and send the profiles amongst others to the CWINDE (2003) hub to receive monthly feedback on the availability and quality of the Doppler radar wind profiles.

Acknowledgments

Hans Beekhuis is gratefully acknowledged for his assistance in optimizing the settings of the Doppler radar and for a pleasant cooperation. The guidance and support of Herman Wessels and Sylvia Barlag are highly appreciated. The punctual reviewing of the manuscript by Sander Tijm and Herman Wessels is greatly appreciated.

Bibliography

- Andersson, T.: 1998, VAD winds from C band Ericsson Doppler Weather Radars. *Meteor. Zeitschrift*, **7**, 309–319.
- Boccippio, D. J.: 1995, A Diagnostic Analysis of the VVP Single-Doppler Retrieval Technique. *J. Atmos. Ocean. Technol.*, **12**, 230–248.
- Browning, K. A. and R. Wexler: 1968, The determination of kinematic properties of a wind field using Doppler radar. *J. Appl. Meteor.*, **7**, 105–113.
- Caya, D. and I. Zawadzki: 1992, VAD Analysis of Nonlinear Wind Fields. *J. Atmos. Ocean. Technol.*, **9**, 575–587.
- Cifelli, R., S. A. Rutledge, D. J. Boccippio, and T. Matejka: 1996, Horizontal Divergence and Vertical Velocity Retrievals from Doppler Radar and Wind Profiler Observations. *J. Atmos. Ocean. Technol.*, **13**, 948–966.
- Collins, W. G.: 2001, The Quality Control of Velocity Azimuth Display (VAD) Winds at the National Centers for Environmental Prediction. *11th Symposium on Meteorological Observations and Instrumentation*, AMS, 317–320.
- CWINDE: 2003, Website of the Coordinated Windprofiler Network in Europe. <http://www.meto.gov.uk/research/interproj/cwinde/>.
- Dlhopolsky, R. and A. Feijt: 2003, An investigation of the representative heights for atmospheric motion vectors. Technical Report TR-249, KNMI.
- Doviak, R. J. and D. S. Zrnić: 1993, *Doppler Radar and Weather Observations*. Academic Press, second edition, 562 pp.
- Eastwood, E.: 1967, *Radar Ornithology*. Methuen, London, 269 pp.
- Foote, G. B. and P. S. DuToit: 1969, Terminal Velocity of Raindrops Aloft. *J. Appl. Meteor.*, **8**, 249–253.

- Gematronik: 2003, Rainbow 3.4 Operator's Manual. Gematronik GmbH., Raiffeneisenstr. 10, 41470 Neuss, Germany.
- Gunn, K. L. S. and R. S. Marshall: 1958, The distribution of size of aggregate snowflakes. *J. Meteor.*, **15**, 452–466.
- Holleman, I. and H. Beekhuis: 2003, Analysis and Correction of Dual-PRF Velocity Data. *J. Atmos. Ocean. Technol.*, **20**, 443–453.
- Holton, J. R.: 1992, *An introduction to dynamic meteorology*. Academic Press, third edition.
- Klein Baltink, H.: 1998, A long-term intercomparison of windprofiler/RASS and tower measurements. *Meteor. Zeitschrift*, **7**, 271–279.
- Koistinen, J.: 2000, Bird migration patterns on weather radars. *Phys. Chem. Earth (B)*, **25**, 1185–1194.
- Lhermitte, R. M. and D. Atlas: 1961, Precipitation motion by pulse Doppler radar. *9th conference on Radar Meteorology*, AMS, 218–223.
- Lindskog, M., H. Järvinen, and D. B. Michelson: 2002, Development of Doppler radar wind data assimilation for the HIRLAM 3D-Var. HIRLAM Technical Report 52, HIRLAM-5 Project.
- Marseille, G. and A. Stoffelen: 2003, Simulation of Wind Profiles from a Space-borne Doppler Wind Lidar. *Q. J. R. Meteorol. Soc.*, in press.
- Matejka, T. and R. C. Srivastava: 1991, An Improved Version of the Extended Velocity-Azimuth Display Analysis of Single-Doppler Radar Data. *J. Atmos. Ocean. Technol.*, **8**, 453–466.
- Matejka, T. J.: 1993, Concurrent Extended Vertical Velocity Azimuth Display (CEVAD). *26th conference on Radar Meteorology*, AMS, 463–465.
- Meischner, P., C. Collier, A. Illingworth, J. Joss, and W. Randeu: 1997, Advanced Weather Radar Systems in Europe: The COST 75 Action. *Bull. Amer. Meteor. Soc.*, **78**, 1411–1430.
- Meulen, J. P. v. d.: 2003, Quarterly reports of the E-AMDAR Quality Evaluation Centre on AMDAR data: 2003-I. EUMETNET report 14, KNMI.
- Passarelli Jr., R. E. and A. D. Siggia: 1983, The Autocorrelation Function and Doppler Spectral Moments: Geometric and Asymptotic Interpretations. *J. Climate Appl. Meteor.*, **22**, 1776–1787.

- Press, W. H., S. A. Teukolsky, W. T. Vetterling, and B. P. Flannery: 1992, *Numerical Recipes in C: the Art of Scientific Computing*. Cambridge University Press, second edition, 994 pp.
- Riley, J. R.: 1999, Radar Returns from Insects: Implications for Meteorological Radars. *29th conference on Radar Meteorology*, AMS, 390–393.
- Rossa, A. M.: 2000, The COST 717 action: use of radar observations in hydrological and NWP models. *Phys. Chem. Earth (B)*, **25**, 1221–1224, also: <http://www.smhi.se/cost717>.
- Schaefer, G. W.: 1969, Radar studies of locust, moth, and butterfly migration in the Sahara. *Proc. Roy. Ent. Soc. Lond., Series C*, **34**, 33 & 39–40.
- Seltmann, J. E. E.: 2000, Clutter versus radar winds. *Phys. Chem. Earth (B)*, **25**, 1173–1178.
- Serafin, R. J. and J. W. Wilson: 2000, Operational Weather Radar in the United States: Progress and Opportunity. *Bull. Amer. Meteor. Soc.*, **81**, 501–518.
- Sigmet: 1998, RVP6 Doppler Signal Processor User's Manual. Sigmet Inc., 2 Park Drive, Westford, MA 01886 USA.
- Sirmans, D., D. Zrnić, and B. Bumgarner: 1976, Extension of Maximum Unambiguous Doppler Velocity by Use of Two Sampling Rates. *17th conference on Radar Meteorology*, Seattle, WA, Amer. Meteor. Soc., 23–28.
- Srivastava, R. C., A. R. Jameson, and P. H. Hildebrand: 1979, Time-Domain Computation of Mean and Variance of Doppler Spectra. *J. Appl. Meteor.*, **18**, 189–194.
- Srivastava, R. C., T. J. Matejka, and T. J. Lorello: 1986, Doppler radar study of the trailing anvil region associated with a squall line. *J. Atmos. Sci.*, **43**, 356–377.
- Tijm, A. B. C. and H. T. Wu: 2000, Assessment of the impact of wind profiler / sodar data on the mesoscale wind analysis in the Netherlands. Technical report, ASWAN final report, KNMI.
- Unden et al., P.: 2002, Hirlam-5 Scientific Documentation. Technical report, Hirlam-5 Project, SMHI, also: <http://hirlam.knmi.nl>.
- Waldteufel, P. and H. Corbin: 1979, On the analysis of single Doppler radar data. *J. Appl. Meteor.*, **18**, 532–542.
- Wessels, H. R. A. and J. H. Beekhuis: 1997, Stepwise procedure for suppression of anomalous ground clutter. *COST-75 Seminar on Advanced Radar Systems*, EUR 16013 EN, 270–277.

- Wilson, J. W., T. M. Weckwerth, J. Vivekanandan, R. M. Wakimoto, and R. W. Russell: 1994, Boundary Layer Clear-Air Radar Echoes: Origin of Echoes and Accuracy of Derived Winds. *J. Atmos. Ocean. Technol.*, **11**, 1184–1206.
- WMO: 1966, *International Meteorological Tables, No. 188, TP. 94*. Secretariat WMO, Geneva, Switzerland.
- 1996, *Guide to Meteorological Instruments and Methods of Observation, No. 8*. Secretariat WMO, Geneva, Switzerland, sixth edition.
- Xin, L. and G. W. Reuter: 1998, VVP Technique Applied to an Alberta Storm. *J. Atmos. Ocean. Technol.*, **15**, 587–592.